AGU PUBLICATIONS

JGR

Journal of Geophysical Research: Atmospheres

RESEARCH ARTICLE
10.1002/2015JD024383

Key Points:
- Two years of atmospheric state data from an instrumented tower on the Ross Ice Shelf are presented
- Stable stratification dominates at this site with the strongest stability for winds $< 4\ m\ s^{-1}$
- Self-organizing maps are used to objectively classify over 100,000 observed temperature profiles

Supporting Information:
- Supporting Information S1

Correspondence to:
J. J. Cassano,
john.cassano@colorado.edu

Citation:
Cassano, J. J., M. A. Nigro, and M. A. Lazzara (2016), Characteristics of the near-surface atmosphere over the Ross Ice Shelf, Antarctica, *J. Geophys. Res. Atmos.*, *121*, 3339–3362, doi:10.1002/2015JD024383.

Received 22 OCT 2015
Accepted 20 MAR 2016
Accepted article online 27 MAR 2016
Published online 12 APR 2016

Characteristics of the near-surface atmosphere over the Ross Ice Shelf, Antarctica

John J. Cassano[1,2], Melissa A. Nigro[1,2], and Matthew A. Lazzara[3,4]

[1]Cooperative Institute for Research in Environmental Sciences, University of Colorado Boulder, Boulder, Colorado, USA, [2]Department of Atmospheric and Oceanic Sciences, University of Colorado Boulder, Boulder, Colorado, USA, [3]Antarctic Meteorological Research Center, Space Science and Engineering Center, University of Wisconsin-Madison, Madison, Wisconsin, USA, [4]Department of Physical Sciences, School of Arts and Sciences, Madison Area Technical College, Madison, Wisconsin, USA

Abstract Two years of data from a 30 m instrumented tower are used to characterize the near-surface atmospheric state over the Ross Ice Shelf, Antarctica. Stable stratification dominates the surface layer at this site, occurring 83% of the time. The strongest inversions occur for wind speeds less than $4\ m\ s^{-1}$ and the inversion strength decreases rapidly as wind speed increases above $4\ m\ s^{-1}$. In summer unstable stratification occurs 50% of the time and unstable conditions are observed in every season. A novel aspect of this work is the use of an artificial neural network pattern identification technique, known as self-organizing maps, to objectively identify characteristic potential temperature profiles that span the range of profiles present in the 2 year study period. The self-organizing map clustering technique allows the more than 100,000 observed potential temperature profiles to be represented by just 30 patterns. The pattern-averaged winds show distinct and physically consistent relationships with the potential temperature profiles. The strongest winds occur for the nearly well mixed but slightly stable patterns and the weakest winds occur for the strongest inversion patterns. The weakest wind shear over the depth of the tower occurs for slightly unstable profiles and the largest wind shear occurs for moderately strong inversions. Pattern-averaged log wind profiles are consistent with theoretical expectations. The log wind profiles exhibit a kinked profile for the strongest inversion cases indicative of decoupling of the winds between the bottom and top of the tower.

1. Introduction

In situ observations of the Antarctic atmosphere are confined primarily to surface observations with very few observations made above the surface. While there are approximately 120 sites that regularly report surface atmospheric conditions, there are only 16 sites that regularly launch radiosondes [*Summerhayes*, 2008]. In addition to these upper air soundings, instrumented towers have been or are located at Plateau Station (79.25°S, 40.5°E) [*Riordan*, 1977], South Pole Station (90°S) [*Hudson and Brandt*, 2005], Dome Concordia (75°S, 123°E) [*Genthon et al.*, 2010, 2013], and Halley Station (76°S, 26°W) [*King and Anderson*, 1988; *King et al.*, 1989; *Anderson*, 2009], providing "above surface" observations. In February 2011, a 30 m instrumented tower was installed on the Ross Ice Shelf at 79.044°S, 170.651°E (Figure 1) to make continuous observations of the near-surface Antarctic atmosphere. This 30 m automatic weather station (AWS) was installed as part of the United States Antarctic Program network of AWS maintained by the University of Wisconsin since 1980 [*Lazzara et al.*, 2012] and will be referred to as the Tall Tower AWS throughout this manuscript.

Instrumented towers have been used widely around the world to study the surface layer and lower portion of the boundary layer [e.g., *Van Ulden and Wieringa*, 1996; *Whiteman et al.*, 1999; *Bowen*, 2000; *Horiguchi et al.*, 2012; *Munoz et al.*, 2013; *Sorbjan and Czerwinska*, 2013]. In addition to these midlatitude surface layer studies, instrumented towers have been used to analyze the surface layer in the polar regions, where snow and ice covered surfaces greatly influence the stability of the near-surface atmosphere [e.g., *Riordan*, 1977; *Persson et al.*, 2002; *Grachev et al.*, 2005; *Hudson and Brandt*, 2005; *Genthon et al.*, 2010; *Grachev et al.*, 2012; *Genthon et al.*, 2013; *Grachev et al.*, 2013; *Van dam et al.*, 2013]. The observations from these high-latitude instrumented towers have provided valuable information about the vertical structure of the near-surface atmosphere in the data sparse polar regions. A brief review of the findings from the data collected at these polar towers is given below.

A 20 m tower was installed on Arctic sea ice during the Surface Heat Budget of the Arctic Ocean (SHEBA) field campaign and collected data for an entire annual cycle. These data indicate stable near-surface conditions dominate for most of the year but near neutral stability is common in the summer and can occur at any time

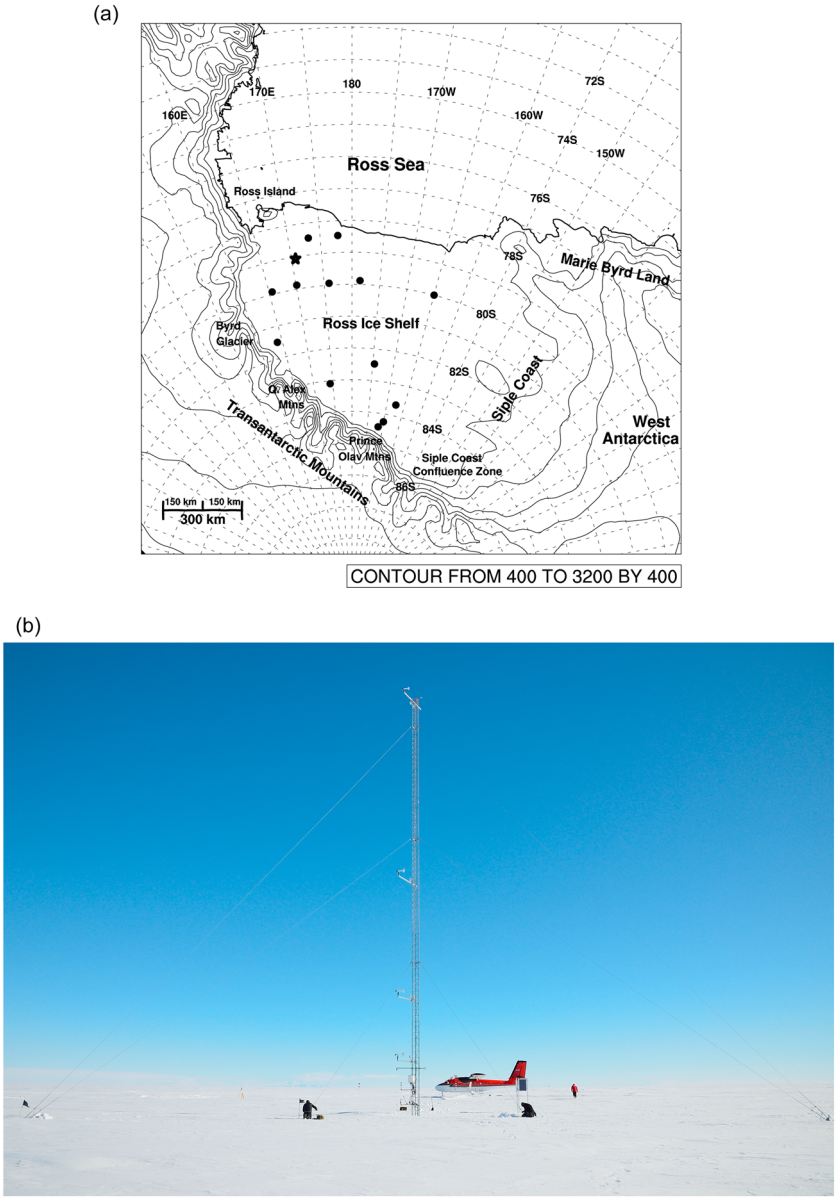

Figure 1. Map of AWS network (black dots) in (a) the vicinity of the Tall Tower (star) AWS and (b) a photograph of the Tall Tower AWS.

throughout the year. During the winter nearly well mixed conditions occur with increased cloud cover or wind speed [*Persson et al*., 2002].

Van dam et al. [2013] used turbulence measurements from a sonic anemometer on an 8 m instrumented tower installed at Summit, Greenland (72°34′N, 38°29′W) to derive the boundary layer depth and compared the results to observations from an acoustic sounder. The results showed that the boundary layer depth varies diurnally and that unstable conditions were present 47% of the time during June 2010.

A 32 m instrumented tower was installed at Plateau Station, Antarctica (79.25°S, 40.5°E) from February to December 1967 to study the near-surface boundary layer structure [*Riordan*, 1977]. Temperature, wind speed, and wind direction were measured at 10 different levels on the tower. It was found that an inversion layer persisted throughout the year and was maintained during periods of diurnal heating and cooling at all levels except for within 1 m of the surface. A diurnal cycle in the strength of the inversion was present during the summer but not during the winter. *Riordan* [1977] found that the inversion at Plateau Station was strongest

for wind speeds of 3 to 6 m s^{-1}. Case studies were used to analyze the large variations in the inversion during the winter season. It was concluded that changes in the surface energy balance, gravity waves, and convergence-induced vertical motion were all contributors to the large temperature changes observed during the winter months.

A 32 m tower has been used at Halley Station to study the near-surface boundary layer. The original tower (75.6°S, 26.7°W) and instrumentation were installed from February to November 1986 as part of the Stable Antarctic Boundary Layer Experiment, which analyzed turbulence and internal gravity waves under conditions of stable stratification [*King and Anderson*, 1988; *King et al*., 1989]. Strong wavelike activity was observed during periods of stable stratification [*King et al*., 1989]. During 2003 through 2008 observations of temperature and wind speed on the 32 m tower (76°S, 26°W) were used to relate the turbulent Prandtl number and the gradient Richardson number under stable conditions [*Anderson*, 2009].

A 22 m instrumented tower was installed upwind of the South Pole Station in 1987 and still remains in operation today. The tower has generally measured temperature, wind speed, and wind direction at the heights of 2 m and 22 m. *Hudson and Brandt* [2005] used the tower data from 1994 to 2003 to understand the relationship between temperature, inversion strength, and wind speed. The authors found that during the summer months, inversions over the 2 to 22 m depth of the tower occur approximately 75% of the time, with strengths of usually less than 1°C and very little to no diurnal cycle. During the winter months, either inversion (with strengths of usually more than 10°C) or isothermal conditions occur over the depth of the tower approximately 90% of the time. It was also determined that the lowest temperatures and the strongest inversion strengths did not occur during periods of calm winds but during periods of winds in the range of 3–5 m s^{-1}. The authors attributed this to the inversion wind, a weak katabatic flow that occurs over the shallow terrain slope in the interior of Antarctica [*Mahrt and Schwerdtfeger*, 1970; *Schwerdtfeger*, 1984; *Hudson and Brandt*, 2005].

A 45 m instrumented tower was installed approximately 700 m away from the Concordia station at Dome Concordia (Dome C), Antarctica in January 2008. *Genthon et al*. [2010] analyzed 3 weeks of 2008 summertime tower observations and concluded that a diurnal cycle exists with convective mixing during the day and a greater than 1°C per 10 m inversion at night. *Genthon et al*. [2013] analyzed the 2009 and 2010 tower observations and concluded that during the summer months a diurnal cycle is observed at the lower levels of the tower but is nonexistent at the upper levels of the tower. The diurnal cycle at the surface is mostly driven by the presence of a shallow surface inversion at night and convective mixing during the day. During the winter months, the observations show a stronger, deeper inversion with a maximum strength of up to nearly 1°C m^{-1} over the height of the tower.

Three of the instrumented towers deployed in the Antarctic, at Plateau Station, South Pole, and Dome C, were located on the high polar plateau and thus have a very different climate than those located on the low-elevation Brunt and Ross ice shelves. The polar plateau locations experience persistent off-continent flow or katabatic winds [*Lettau*, 1969; *Parish and Bromwich*, 1987, 2007], strong surface inversions [*Phillpot and Zillman*, 1970], extremely low surface temperatures [*Comiso*, 1994], low cloud fraction [*King and Turner*, 1997; *Bromwich et al*., 2012], and low precipitation rates [*Bromwich*, 1988]. These observations have greatly improved our knowledge of the near-surface layer over the interior of the Antarctic continent. Conversely, the work presented here characterizes the near-surface atmosphere over the Ross Ice Shelf, Antarctica, a region located farther north and at a lower elevation than the stations on the polar plateau. The Ross Ice Shelf experiences marine influences from passing synoptic scale and mesoscale cyclones [*Jones and Simmonds*, 1993], as well as weaker surface inversions [*Phillpot and Zillman*, 1970], warmer surface temperatures [*Comiso*, 1994], higher cloud fraction [*King and Turner*, 1997; *Bromwich et al*., 2012], and higher precipitation rates [*Bromwich*, 1988] than the regions of East Antarctica. The observations from the Tall Tower AWS thus offer near-surface observations from a very different climatic regime than the towers located on the polar plateau.

In this paper, two years (February 2011 to January 2013) of data from the 30 m Tall Tower AWS are used to characterize the near-surface atmospheric state over the Ross Ice Shelf. Details of the data and analysis methods used for this research are presented in sections 2 and 3. Section 4 identifies the mean characteristics of the potential temperature and wind profiles over the lowest 30 m of the atmosphere over the Ross Ice Shelf on an annual, seasonal, and diurnal basis. A novel aspect of this work is the use of an artificial neural network pattern identification technique, known as self-organizing maps (SOMs), to objectively identify characteristic potential temperature profiles that span the range of profiles present in the more than 100,000 profiles

observed over the 2 year study period. The frequency of occurrence of each pattern is determined on an annual and seasonal basis and relationships between winds and potential temperature profiles are determined. The paper concludes with a discussion of how the near-surface atmosphere over the Ross Ice Shelf compares with other lower atmosphere measurements made in the polar regions and prospects for future surface and boundary layer studies at the Tall Tower site.

2. Data

The primary data for the work presented below are 10 min instantaneous observations of temperature, pressure, and wind made at the Tall Tower AWS site at 79.044°S, 170.651°E (Figure 1). This AWS is located on the Ross Ice Shelf at an elevation of 55 m. Flat and uniform surface conditions dominate this region. The nearest topographic features are Minna Bluff 85 km toward the west northwest, the Transantarctic Mountain range 170 km to the west, which runs roughly northwest to southeast, and the eastern tip of Ross Island located 170 km to the north.

The Tall Tower AWS was installed in February 2011 with six levels of instrumentation. Unlike all previous Antarctic AWS installed by the University of Wisconsin [*Lazzara et al*., 2012], which are at most several meters tall, this AWS is 30 m tall and thus is referred to as the Tall Tower AWS. During the time period of this study, February 2011 to January 2013, the AWS measured temperature using R. M. Young platinum resistance temperature devices at 0.85, 1.83, 3.75, 7.25, 14.75, and 29.75 m, humidity using Vaisala HMP45C-L at 7.25 and 29.75 m, wind speed using an R. M. Young Wind Sentry cup anemometer at 1.34 m, wind speed and wind direction using R. M. Young aerovanes at 3.75, 7.25, 14.75, and 29.75 m, pressure using a Vaisala pressure sensor at 2.3 m, surface height using a Campbell Scientific acoustic depth gauge at 3.2 m, and net longwave and shortwave radiation using a Kipp and Zonen CNR2-L at 29.75 m. The location of Tall Tower receives approximately 0.5 m of snow accumulation per year and the instruments are periodically raised to keep all instrumentation above the snow surface, although none of the instruments were raised during the 2 year period of this study. As a result the instrument height to the surface decreased by 1.1 m from February 2011 to January 2013. This change in height will result in a downward trend in temperature, due to the persistent inversion conditions at this site, and a weakening of wind with time, but no corrections or adjustments to the observations were made to account for the changing instrument height relative to the ground. Note that all heights listed above are the mean heights of the instruments over the 2 year study period. The Antarctic Meteorological Research Center AWS website (http://amrc.ssec.wisc.edu/) provides information about specific instrumentation heights and the servicing performed on the stations for a given year.

The analysis in this paper focuses on the temperature and wind speed measurements from the Tall Tower AWS. The R. M. Young platinum resistance temperature devices have a manufacturer stated accuracy of ±0.3°C. The cup anemometer, at a height of 1.34 m, has a manufacturer stated accuracy of ±0.5 m s^{-1} while the aerovanes, at 3.75, 7.25, 14.75, and 29.75 m, have a manufacturer stated accuracy of ±0.3 m s^{-1}. It is assumed that individual measurements may have errors up to the stated ranges listed above but that these errors are random and thus over the large number of observations considered in this work are negligible in the mean. Possible nonrandom radiation induced temperature errors are discussed below.

Since much of the work presented below focuses on vertical temperature gradients it is important to carefully assess if there are any persistent biases between the temperature measurements at the various tower levels. Unfortunately, due to the remote location of this site and logistic challenges during the deployment of the tower, no intercomparison of the temperature sensors prior to deployment was completed. In order to determine if there are any biases in the vertical potential temperature differences between various tower levels, all 54,047 observations when the wind speed at 3.75 m was greater than 5 m s^{-1} were analyzed. These moderate to strong wind speed cases were analyzed since turbulence should be well developed over the depth of the tower, and thus, the potential temperature should vary in a uniform manner with height. Comparison of the median potential temperature difference between all possible pairs of tower levels suggested that the temperature at 1.83 m and 3.75 were biased relative to the other tower levels. Figure 2 (solid lines) shows the potential temperature difference for all tower levels relative to the measurements at 29.75 and 14.75 m. These profiles do not vary uniformly with height, as would be expected under turbulent conditions. Using the observations at 29.75, 14.75, and 0.83 m a linear regression was performed on the data relative to log height (Figure 2b). Based on this linear regression a correction of −0.09°C (+0.08°C) is applied to all potential

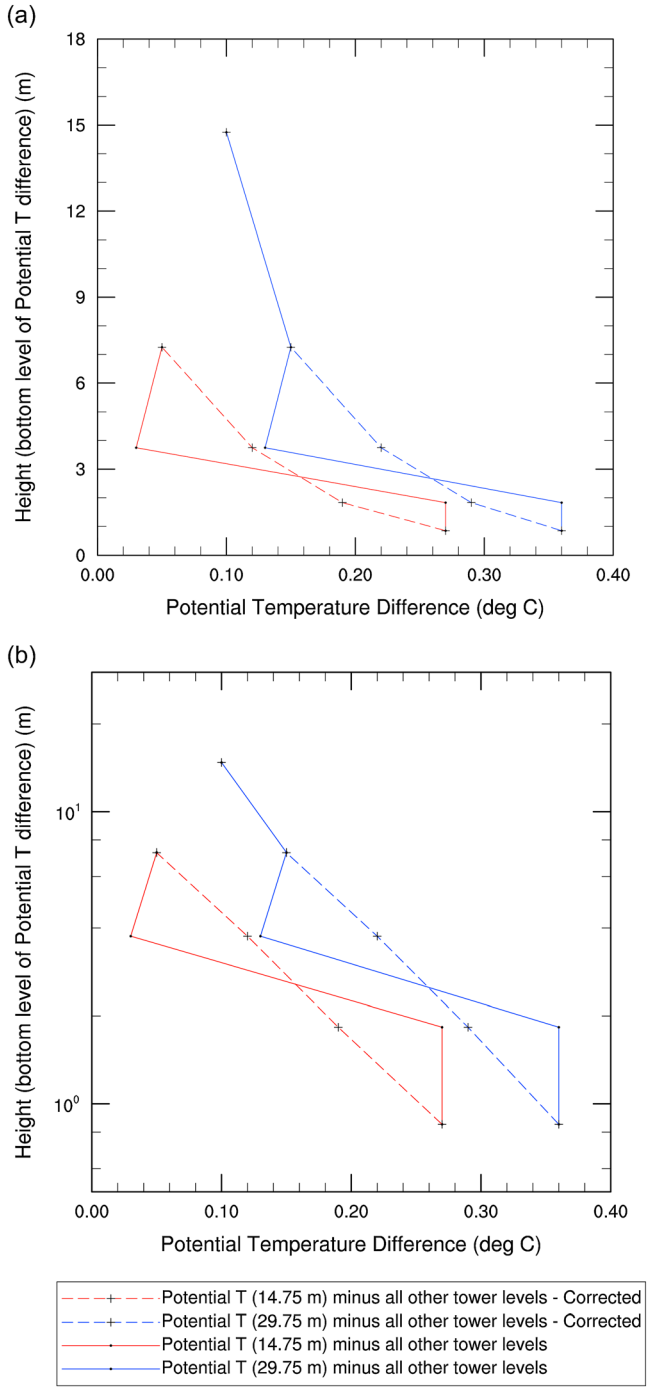

Figure 2. Profiles of potential temperature difference between 29.75 m tower level and all other tower levels (blue) and between 14.75 m tower level and all other tower levels (red) for the uncorrected (solid) and corrected (dashed) Tall Tower data. Data plotted versus height in Figure 2a and versus log height in Figure 2b.

temperature observations at 3.75 m (1.83 m) resulting in a more uniform change of potential temperature with height (Figure 2, dashed lines). These corrected data are used throughout the remainder of the paper.

As discussed in *Genthon et al.* [2011], radiation errors in temperature measurements made at Antarctic AWS sites that do not use aspirated radiation shields can be an issue during weak wind conditions in the summer. For the work presented in this paper, the instantaneous 10 min temperature observations were quality controlled for radiation errors. Temperature observations were flagged if the temperature increased by more than 1°C between two 10 min observations, the winds were less than 3 m s^{-1}, and the sun was above the horizon. All of the flagged temperatures were manually analyzed to determine if the temperature increase was within the temperature variability of that day. If the increase in temperature was within the temperature variability of the day, then the data point was not removed. If it was outside of the temperature variability, then the observation was removed from the data set. We also removed all data points (55 in total) when the air temperature exceeded 0°C as this is highly unlikely given the permanent snow surface at this site. It is possible that this quality control procedure is not identifying all radiation errors in the temperature measurements. Because the radiation errors will decrease with increased wind speed, radiation errors are likely largest at the lowest tower level and thus will bias vertical temperature gradient calculations toward weaker stability. The impact of this is discussed in the results and conclusions below.

The observational data set consisted of a total of 103,982 temperature observations. Of these observations, 721 (0.7%) were rejected for either missing data (the instrument did not record an observation) or were removed during the quality control process. The wind speed and wind direction observations were quality controlled for instances when the cup anemometers and aerovanes were frozen. The wind speed and wind direction observations were manually analyzed for removal when either the wind speed was zero for longer than a day or the wind direction was constant for longer than a day. The cup anemometer, which is located closest to the surface, experienced

the most frequent problems with freezing and was considered frozen during all of June 2011 and April 2012 through September 2012.

For the work presented here, the summer is defined as December and January, autumn as February, March, and April, winter as May, June, July, and August, and spring as September, October, and November. This seasonal definition was chosen for consistency with previous Antarctic research [*Seefeldt and Cassano*, 2008, 2012; *Nigro and Cassano*, 2014].

3. Methods

Statistics such as mean, median, and percentile values are calculated for various observations from the Tall Tower AWS to provide a characterization of the seasonal and annual range of conditions observed at this site. These statistics are calculated using the 10 min quality controlled AWS observations described above.

To more fully characterize the variability in the 100,000+ 10 min Tall Tower AWS observations we use the method of SOMs. The SOM technique employs a neural network algorithm that uses unsupervised learning to determine generalized patterns in data and reduces the dimensions of large data sets by grouping similar data records together and organizing them into a two-dimensional array, referred to as a map or master SOM. As a result, large, multidimensional data sets are reduced to more easily interpreted forms. Used in this way the SOM algorithm may be considered a clustering technique, but unlike other clustering techniques, the SOM method does not need a priori decisions on data distribution and is instead trained through an iterative process. The final two-dimensional array of patterns (master SOM) represents the full continuum of states represented in the training data set. This array is organized such that similar patterns are located in the same portion of the master SOM with dissimilar patterns on opposite corners of the array. This organization of the final patterns allows for easier analysis of interpattern relationships. *Kohonen* [2001] provides a detailed description of the SOM algorithm and *Hewitson and Crane* [2002] provide additional information on the application of the SOM technique to climate data. *Cassano et al*. [2015] review many of the issues that need to be considered when using the SOM technique.

For this study, the SOM algorithm was trained using 100,000+ instantaneous 10 min potential temperature anomaly profiles from the Tall Tower AWS. For each 10 min profile the average potential temperature over the depth of the tower was calculated and subtracted from the observed potential temperature at each tower level to give the potential temperature anomaly profile. The use of potential temperature anomaly preserves the shape of the profile without retaining the absolute magnitude of the potential temperature and ensures that the SOM training focuses on the shape of the profile and the magnitude of the potential temperature change between tower levels rather than on the absolute magnitude of the potential temperature. This allows for robust classification of potential temperature profiles over the entire annual cycle.

As discussed in *Cassano et al*. [2015, and references therein], a critical decision that needs to be made when applying the SOM technique is the number of patterns to be defined by the algorithm. The advantage of using a relatively small number of patterns is that clearly distinguishable differences in features can be seen in each pattern and a relatively small SOM is easy to visualize. The disadvantage of using a small number of patterns is that each pattern can become too generalized and not allow for clear identification of features relevant to relatively rare events. The use of larger SOM arrays provides for finer differences between each pattern and can help separate patterns with relatively similar features but important small-scale differences. The disadvantages of using a large SOM array include difficulty in visualizing all of the patterns and issues of representativeness of the patterns caused by the small numbers of events corresponding to each pattern. Many previous SOM-based atmospheric studies have used a 7×5 SOM that represents the training data with 35 patterns. For this work we trained SOMs ranging from 4×2 (8 patterns) to 7×5 (35 patterns) but found that a 5×6 (30 patterns) SOM adequately captured the range of potential temperature profiles present in the training data while not creating patterns that were too similar (Figure 3).

Because the SOM technique is still relatively unknown to many scientists it is useful to compare the SOM technique to a better known data discretization technique—a digital elevation model (DEM). A DEM provides a gridded representation of continuously varying topography and the SOM is similar in that it provides a gridded representation of a continuously varying data space, which in this paper is defined by potential temperature anomaly profiles observed over a 2 year period at a 30 m Tall Tower AWS on the Ross Ice

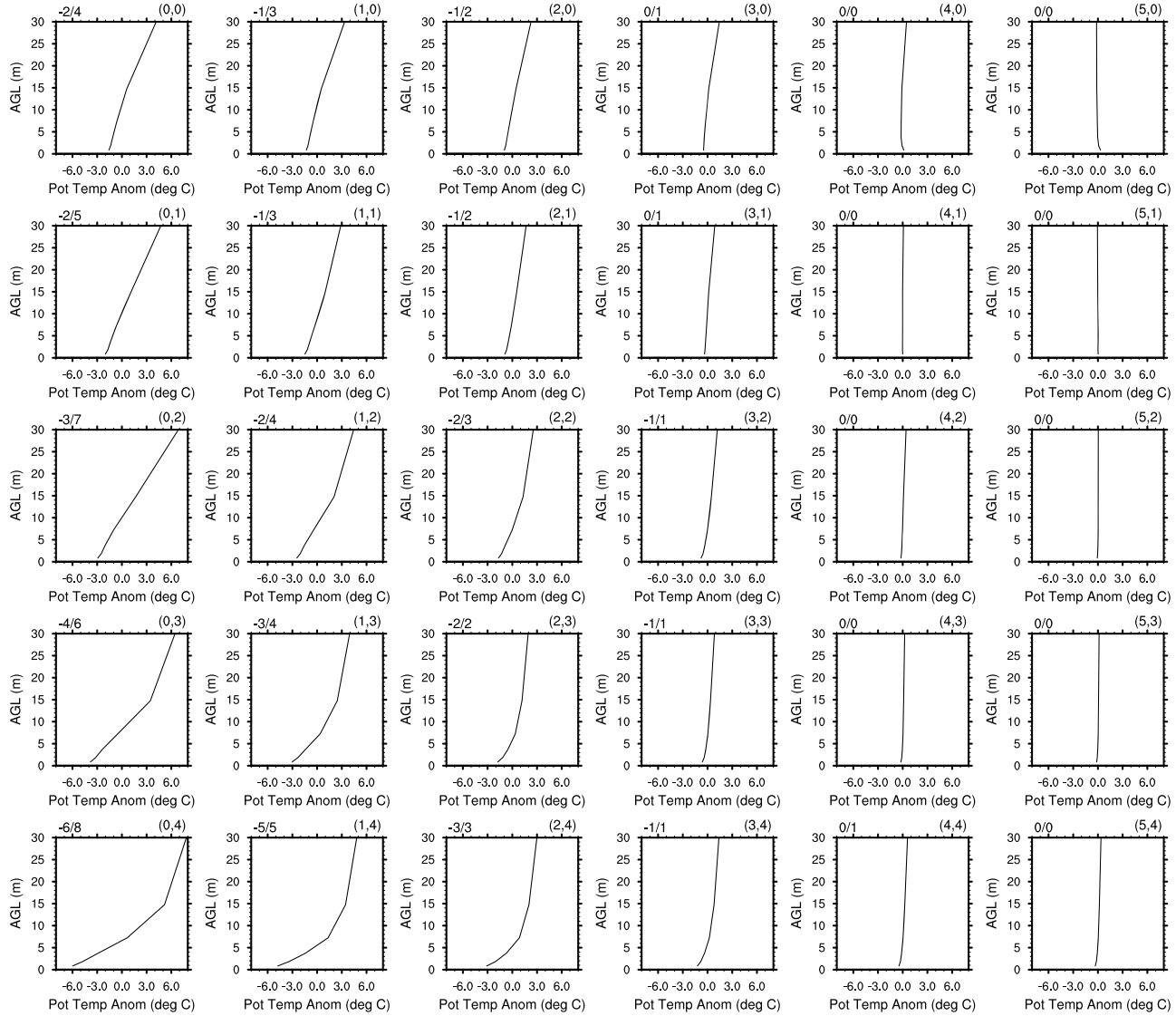

Figure 3. Self-organizing map (SOM) of potential temperature anomaly profiles for Tall Tower observations from February 2011 to January 2013. Numbers listed at the top left of each SOM pattern indicate the maximum and minimum potential temperature anomaly over the depth of the profile. The numbers in parenthesis listed at the top right of each SOM pattern indicate the SOM column and row number.

Shelf. If the DEM grid is shifted in space the elevations defined on the DEM will differ but will still represent the same topography. Similarly, multiple SOMs can be created from the same training data that differ in the exact details of their individual patterns but still represent the range of conditions within the training data space. The level of discretization of the data space in a SOM is determined based on the number of SOM patterns that the user defines when training the SOM. This is similar to varying the horizontal resolution of a DEM grid. A small SOM corresponds to a coarse resolution DEM, while a large SOM corresponds to a high-resolution DEM. In both cases the underlying data are unchanged and only the level of detail evident in the gridded data set changes. As with a high-resolution DEM where adjacent grid points likely have similar elevations a large SOM will result in adjacent patterns that are similar due to their close proximity in data space. Depending on the intended application this may be a useful attribute of the SOM and needs to be considered carefully when training the SOM. *Cassano et al.* [2015] discuss some of the factors that need to be considered when choosing a SOM size. As with a high-resolution DEM a large SOM can be used to identify both fine scale details by looking at pattern-to-pattern changes in the SOM as well as view broader patterns present in the data by looking across large portions of the SOM space. The analysis presented in this paper

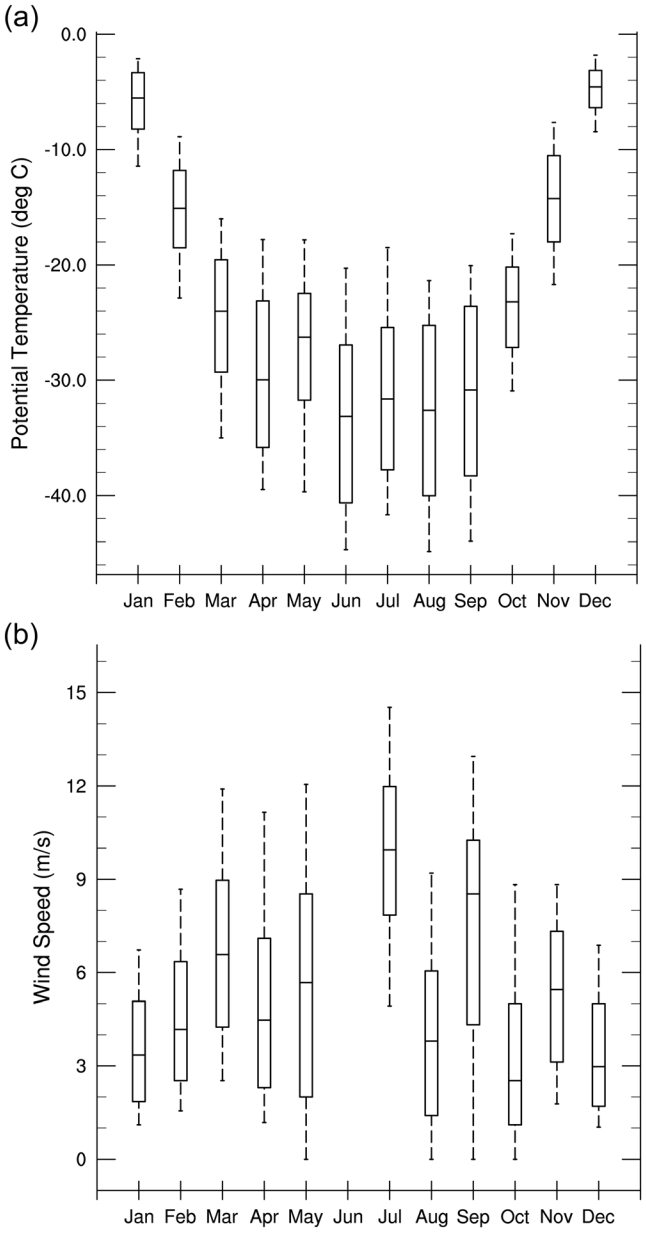

Figure 4. Monthly median (center line), 25th and 75th percentile (edge of boxes), and 10th and 90th percentile (whiskers) (a) potential temperature at 0.85 m and (b) wind speed at 1.34 m. All data are for the period February 2011 to January 2013. Due to a large fraction of missing wind speed data for June no values are plotted for this month.

seeks to resolve the details of over 100,000 potential temperature profiles in a relatively compact manner. To do this we have chosen to use a 30 pattern (5 × 6) SOM to depict the details of this large data space, but much of our analysis will focus on a broader view of the SOM and will primarily discuss features that vary across distant portions of the SOM space.

Once the master SOM has been defined, individual potential temperature anomaly profiles can be mapped to the SOM. Mapping data to the SOM require that each sample be associated with a single pattern on the master SOM. This is accomplished by finding the master SOM pattern that minimizes the squared difference between the potential temperature anomalies that define the SOM pattern and the potential temperature anomalies in the sample of interest. By repeating this mapping for all of the samples in the data set a list of samples associated with each SOM pattern is created. This list can be used to calculate the frequency of occurrence of each pattern over the entire data set or for subsets of the data set (such as individual seasons). The list of samples associated with each pattern can also be used to composite other variables onto the SOM patterns. For example, the median wind speed for all 10 min observations that correspond to an individual SOM pattern can be calculated allowing for analysis of relationships between a particular type of potential temperature anomaly profile and the winds observed when those types of profiles are occuring.

4. Results

4.1. Mean Near-Surface Atmospheric State

The observed monthly median, 10th, 25th, 75th, and 90th percentile potential temperatures at 0.85 m are shown in Figure 4a. During the 2 year observing period at Tall Tower, the maximum observed 0.85 m potential temperature was 2.0°C on 26 December 2011 and the minimum was −56.8°C on 21 September 2011. The monthly median potential temperature observations show the expected annual cycle of warmer temperatures during the austral summer and colder temperatures during the austral winter, with an annual range of monthly median temperatures of approximately 28°C. The 2 years of data from the Tall Tower AWS reveal the

characteristic coreless winter of the Antarctic [*King and Turner*, 1997] when temperatures remain consistently low for several months. Figure 4a also shows that the austral winter months have a larger intramonth variability than the summer months. This is likely due to the fact that during the winter months strong surface inversions frequently develop over the Ross Ice Shelf resulting in very cold surface temperatures. Periods of strong winds, which increase turbulence, enhance near-surface vertical mixing of the warmer temperatures from aloft, resulting in large temperature changes during the winter months [*Schwerdtfeger*, 1977]. In addition, strong temperature advection and changes in cloud cover, resulting in large changes in the surface radiation budget, also cause large changes in near-surface temperature in the winter. *Hudson and Brandt* [2005] also documented these phenomena using temperature observations from the Amundsen-Scott South Pole Station.

The observed monthly median, 10th, 25th, 75th, and 90th percentile wind speeds at 1.34 m are shown in Figure 4b. The maximum 1.34 m wind speed observed at Tall Tower during the 2 year observing period was 21.4 m s^{-1} on 9 April 2011. The monthly median wind speed observations show that in general, stronger winds occur during the nonsummer months (with the exception of October). The stronger nonsummer winds are consistent with previous studies of the winds over the Ross Ice Shelf [e.g., *Parish et al*., 1994; *Nigro and Cassano*, 2014] and are due to the fact that the Tall Tower AWS is located in a region of the Ross Ice Shelf that is impacted by features such as katabatic drainage, the Ross Ice Shelf airstream (RAS), and the pressure gradient associated with the semipermanent synoptic-scale low-pressure system located off the coast of West Antarctica (see references in *Nigro and Cassano* [2014]), which are all stronger during the nonsummer months.

The potential temperature exhibits a diurnal cycle in all seasons except winter (May, June, July, and August (MJJA)) (Figure 5) that is largest at 0.85 m and is generally half as large at 29.75 m. On an annual basis the amplitude of the diurnal cycle ranges from 0.5°C (MJJA) to 4.0°C (December and January (DJ)) at 0.85 m. At 29.75 m the amplitude of the diurnal cycle ranges from 0.4°C (MJJA) to 2.4°C (DJ). The error bars in Figure 5 show the variability (±1 standard deviation) of the temperature during each 30 min period during the day. Other than at the two lowest tower levels during DJ the amplitude of the diurnal cycle is generally less than the temperature variability at a given time of day. This indicates that there is no statistically robust diurnal cycle other than during the summer at this site.

The vertical potential temperature difference (referred to as the inversion strength hereafter) over the height of the tower is a defining characteristic of the near-surface atmospheric state. We note that our use of the term inversion strength does not refer to the total inversion strength, since surface-based inversions may be several hundred meters deep, and instead refers only to the inversion strength over the depth of the tower. Positive values of the vertical potential temperature difference indicate statically stable conditions, while negative values indicated statically unstable conditions. The frequency of different inversion strengths between 29.75 m and 0.85 m (referred to as over the height of the tower in the remainder of the paper), in 0.5°C intervals, is shown in Figure 6. Over the entire 2 year period (Figure 6a) stable stratification dominates, occurring 83% of the time. The most common potential temperature difference is between 0 and 0.5°C and occurs 27% of the time. The maximum inversion strengths observed exceed 25°C. The second most common potential temperature difference is −0.5 to 0°C and occurs 15% of the time. Conditions that are more unstable than this occur very rarely resulting in a potential temperature difference distribution that is skewed heavily toward stable stratification. Given that individual temperature measurements have an accuracy of ±0.3°C the uncertainty in the temperature difference between pairs of tower levels is ±0.6°C. As discussed above, this level of uncertainty is assumed to be a random error and thus over the large number of observations considered here will not alter the inversion strength distributions shown in Figure 6, although radiation errors may result in reduced inversion strength or unstable conditions during light wind conditions, although these errors are an issue only during the summer [*Genthon et al*., 2011].

As expected, given the pronounced seasonal cycle of incoming solar radiation [*King and Turner*, 1997], the inversion strength over the height of the tower also exhibits a pronounced seasonal cycle. Unstable conditions with a difference of −0.5 to 0°C are the most common (42%) potential temperature difference during the austral summer months of DJ (Figure 6b). At this time of the year stable conditions occur 50% of the time and the maximum inversion strength exceeds 11°C. These results should be viewed as qualitatively correct although radiation errors may result in weaker stability being indicated than is actually occurring. Stable

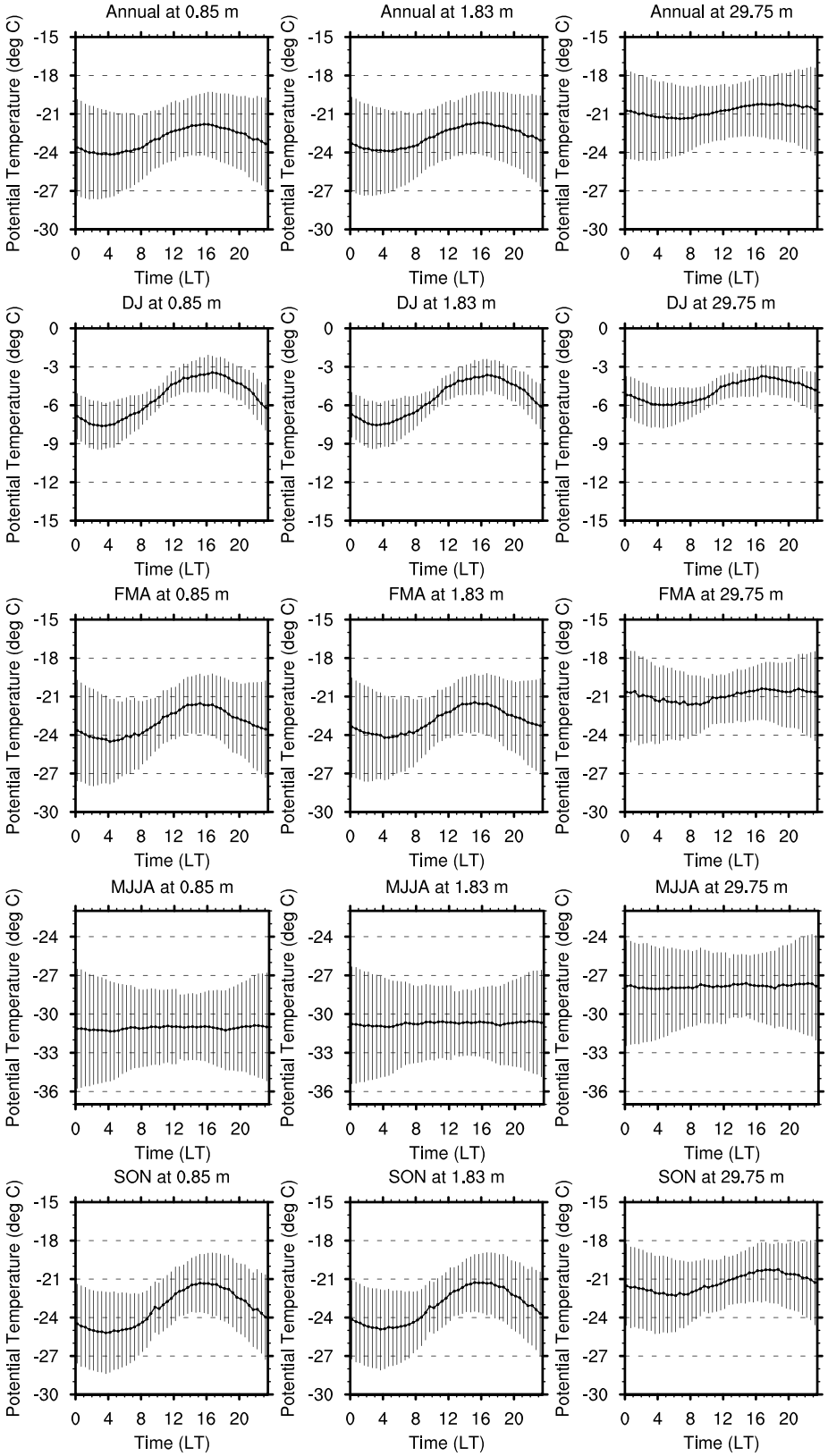

Figure 5. Mean diurnal cycle of (top row) annual and seasonal ((second row) DJ, (third row) FMA, (fourth row) MJJA, and (fifth) SON) potential temperature at 0.85 m (left column), 1.83 m (middle column), and 29.75 m (right column). Error bars show ±1 standard deviation of the potential temperature for each 30 min period during the day.

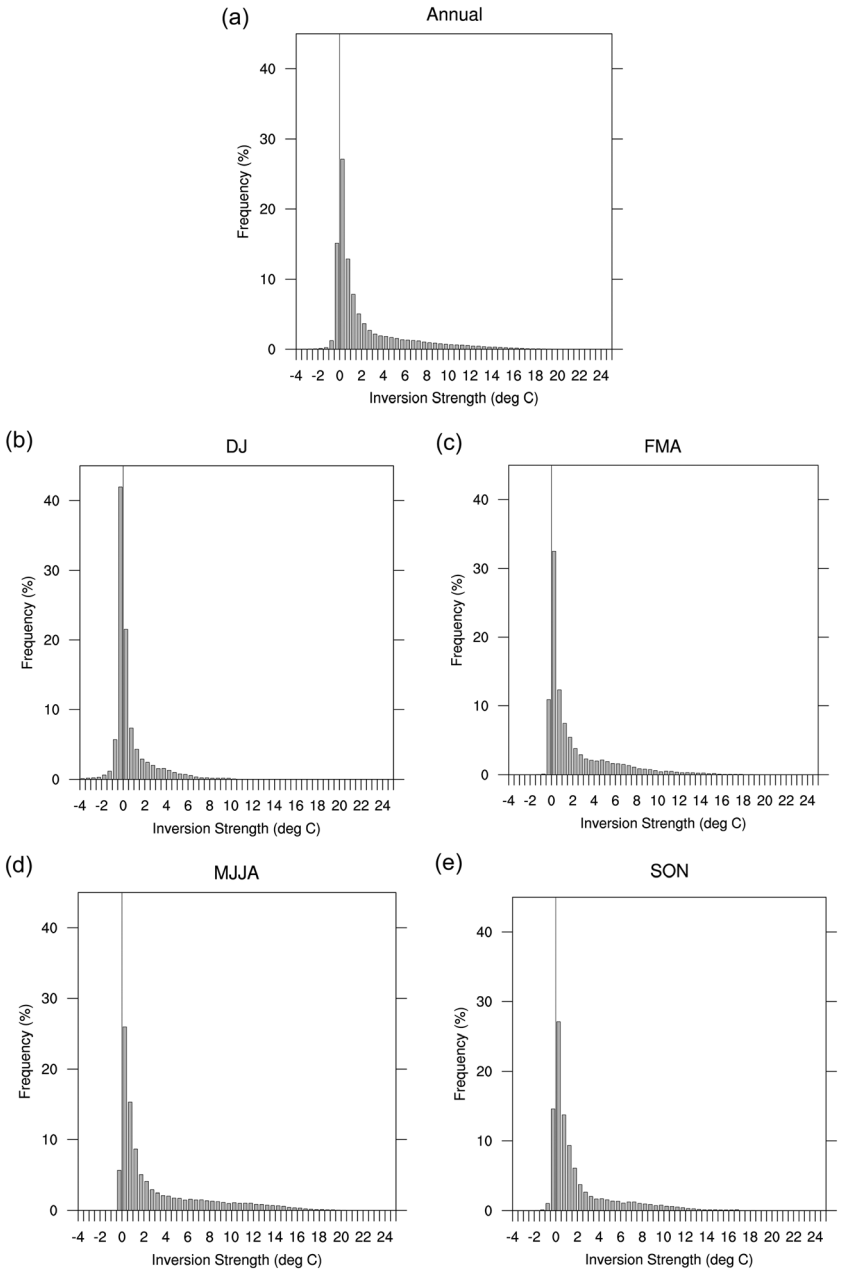

Figure 6. Histogram of (a) annual and seasonal ((b) DJ, (c) FMA, (d) MJJA, and (e) SON) inversion strength over the depth of the tower (29.75 to 0.85 m). The thin vertical line marks the 0°C inversion strength.

stratification dominates the remaining three seasons (Figures 6c to 6e; February, March, and April (FMA)—89%, MJJA—94%, and September, October, and November (SON)—84%) although unstable conditions are also observed in every season. In all seasons the inversion strength is skewed toward positive (stable) values.

The diurnal cycle of inversion strength between the two lowest levels (1.85 and 0.85 m) of the Tall Tower AWS and over the entire depth of the AWS are shown in Figure 7. The inversion strength over these two depths is shown since the vertical potential temperature gradient is typically largest near the surface and decreases over greater depths. In the annual mean stable conditions (positive inversion strength) persist throughout the diurnal cycle between the lowest two tower levels (Figure 7a) and over the entire depth of the tower (Figure 7b). Over the diurnal cycle the annual mean inversion strength is smallest (from approximately 0.1 to 0.3°C) between the two lowest tower levels and increases to 1.5 to 3.0°C over the depth of

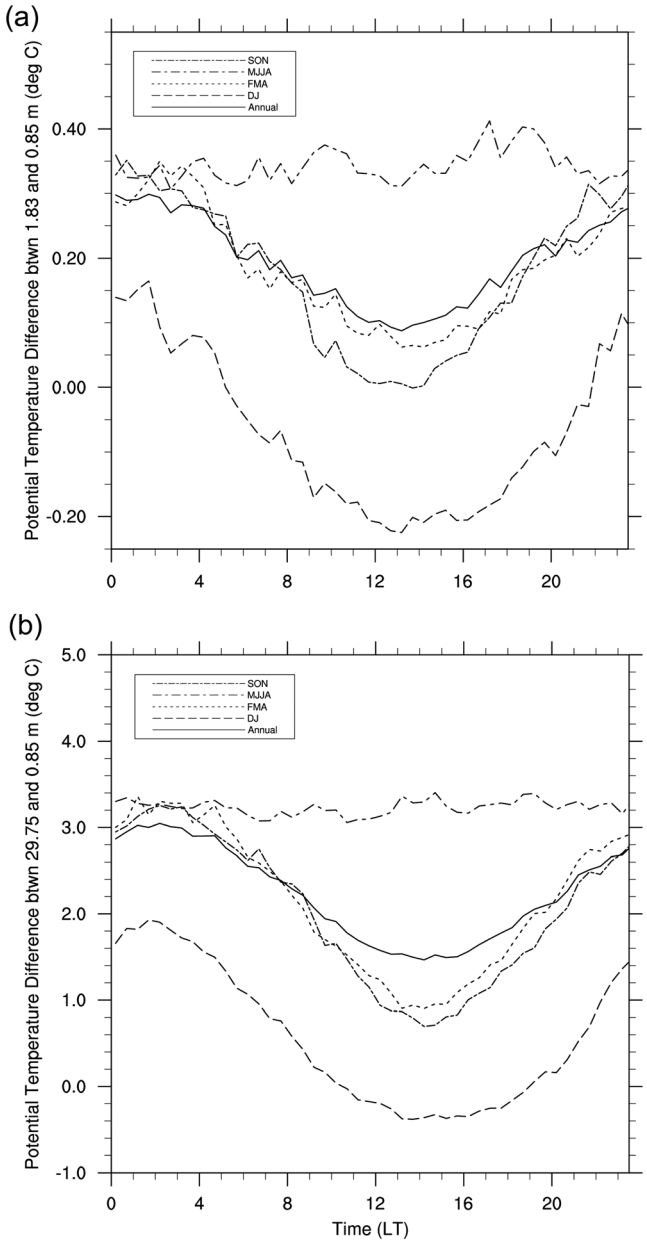

Figure 7. Mean diurnal cycle of potential temperature difference between (a) the lowest two tower level (1.83 and 0.85 m) and (b) over the depth of the tower (29.75 to 0.85 m) for annual (solid line) and seasonal (DJ (dashed line), FMA (dotted line), MJJA (dash dot line), and SON (dash dash line)) periods.

the tower. Consistent with the mean diurnal cycle of potential temperature (Figure 5) the weakest stratification occurs in the afternoon (between 13 and 16 LT) and the strongest stratification occurs overnight (between 01 and 03 LT).

In the seasonal mean, unstable stratification (−0.2 to 0.0°C) occurs over the two lowest tower levels between 05 and 22 LT during the summer but is confined to the late morning through evening (11 to 19 LT) over the height of the tower (Figure 7). Stable stratification reaches a mean summer maximum of 1.9°C over the depth of the tower between 02 and 03 LT. Stable conditions with little daily variability occur in winter over all tower levels. During the winter, the mean inversion strength is between 0.3 and 0.4°C between the two lowest tower levels while the inversion strength varies from 3.1 to 3.4°C over the depth of the tower. During autumn and spring the inversion strength once again exhibits a diurnal cycle with neutral to slightly stable conditions (0 to 0.35 K) occurring between the two lowest tower levels, while stable stratification (0.7 to 3.4 K) occurs throughout the mean diurnal cycle over the depth of the tower.

The sign and strength of the inversion varies strongly with wind speed (Figure 8). Over the entire 2 year period the largest median (up to 3 K) and 90th percentile (up to 12 K) inversion strength over the depth of the tower occurs for wind speeds of less than 4 m s^{-1}. The median inversion strength weakens slightly at lighter wind speeds and decreases rapidly with wind speeds greater than 4 m s^{-1}. The median inversion strength decreases to less than 1°C for wind speeds greater than 6 m s^{-1}. The range (10th to 90th percentile) of inversion strengths for a given wind speed ranges from −1°C to 12°C for wind speeds less than 4 m s^{-1} and narrows considerably as the wind speed increases.

Seasonally, the largest median and 90th percentile inversion strengths occur for wind speeds < 4 m s^{-1} (Figures 8b to 8e). In summer the median conditions are near neutral to slightly stable for all wind speeds, while the 10th percentile values are unstable for all wind speeds (Figure 8b). As discussed above, radiation errors during the summer, when winds are weak, may result in erroneous unstable conditions being measured. Evidence for this is seen in the unstable conditions indicated by the 10th percentile inversion strength values in summer for wind speeds less than 4 m s^{-1}. However, the fact that unstable conditions are observed

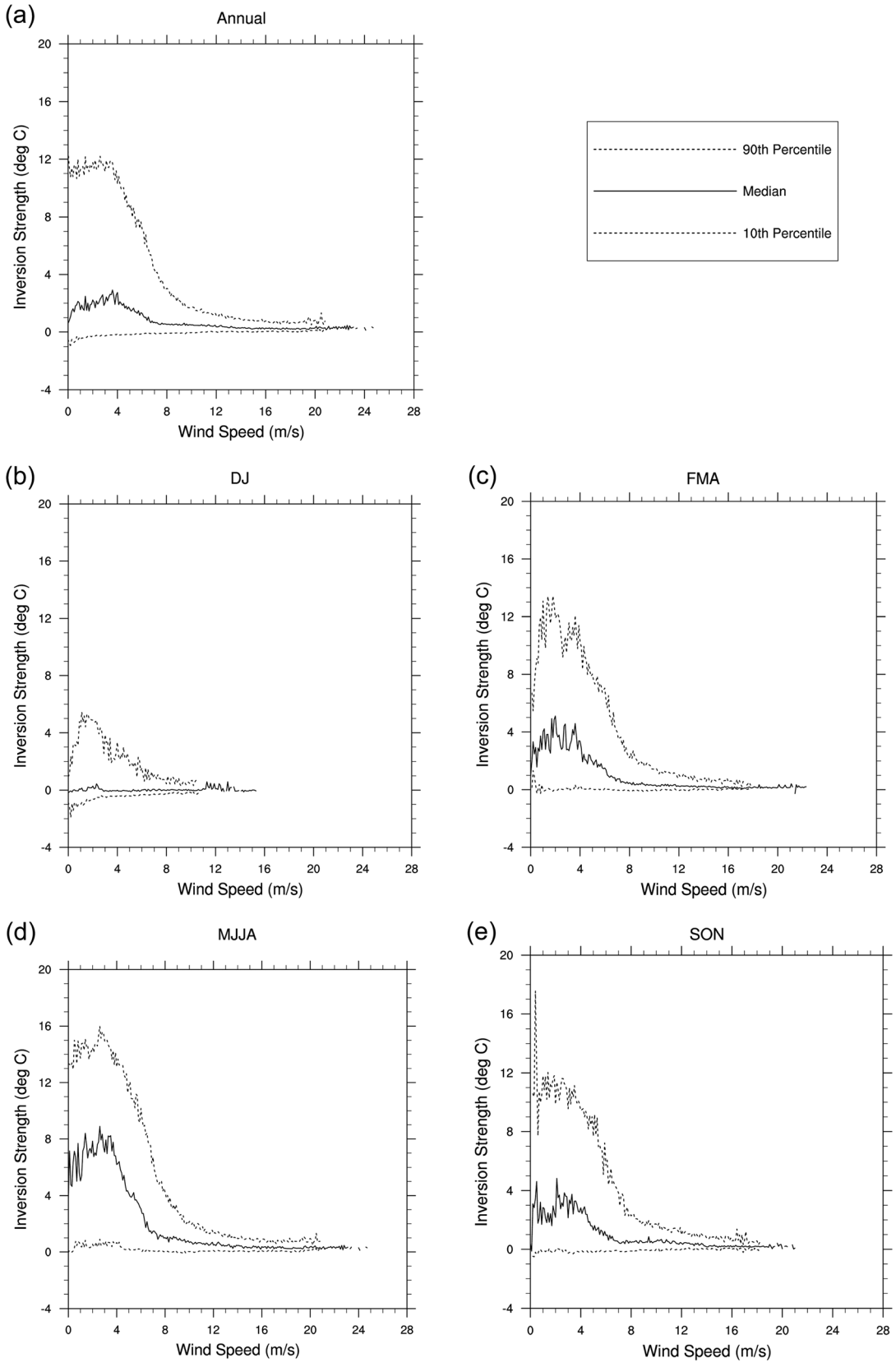

Figure 8. Relationship between median (solid line) and 10th and 90th percentile (dashed lines) inversion strength over the depth of the tower (29.75 to 0.85 m) and average wind speed over the depth of the tower for (a) annual and seasonal ((b) DJ, (c) FMA, (d) MJJA, and (e) SON) periods.

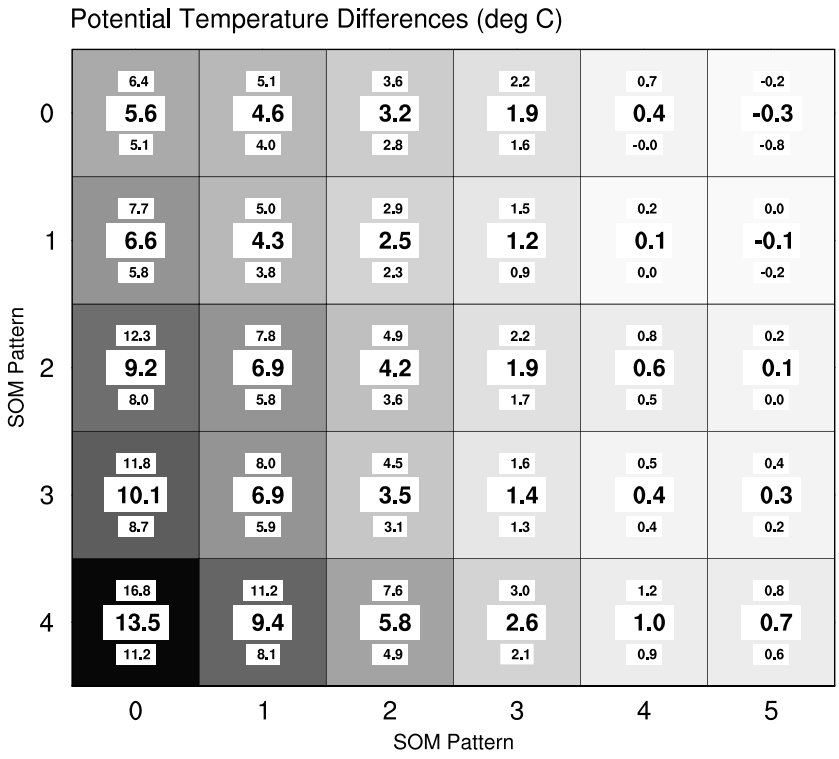

Figure 9. Median, 10th, and 90th percentile inversion strength over the depth of the tower (29.75 to 0.85 m) for each SOM pattern. Darker shading indicates larger median values. The 10th and 90th percentile values are listed below and above the median values, respectively.

in the 10th percentile inversion strength values for stronger wind speeds does suggest that unstable conditions do actually occur at this site in summer and are not purely an artifact of radiation errors. In summer 90th percentile inversion strengths reach maximum values over 5°C for wind speeds of 1 to 2 m s^{-1}. In winter the median (90th percentile) inversion strength ranges from 5 to 9°C (13 to 16°C) for wind speeds less than 4 m s^{-1} and fall rapidly as wind speed increases (Figure 8d). During the winter the 10th percentile inversion strength is near neutral for all wind speeds. In autumn and spring the median inversion strength ranges from 2 to 5°C for wind speeds less than 5 m s^{-1} (Figures 8c and 8e) and decrease rapidly as wind speed increases above 4 m s^{-1}. The 10th percentile inversion strengths vary from slightly unstable for the lightest wind speeds to near neutral for all other wind speeds.

4.2. SOM Analysis of Near-Surface Atmospheric Profiles

The SOM technique was used to identify the range of potential temperature profiles that are present in over 100,000 10 min tower observations collected during the 2 year study period (Figure 3). The output from the algorithm is a 5 × 6 grid of potential temperature anomaly profiles, known as a SOM, that are arranged such that similar patterns are close to each other on the grid. In general, stable profiles are found on the left side of the SOM with near neutral profiles on the right side of the SOM. The stratification also increases from the top to the bottom of the SOM. The similarity between profiles can be shown graphically using a Sammon map, with the distance between plotted points on the Sammon map representing the squared difference between the data points in a given pair of profiles (Figure S1 in the supporting information). The Sammon map for the SOM of potential temperature profiles indicates that the profiles on the right side of the SOM are nearly identical, while the profiles on the left side of the SOM differ most from their neighboring patterns and this is consistent with a visual inspection of Figure 3.

As described in the methods section, each observation from the Tall Tower AWS can be associated with the single best matching pattern on the SOM, resulting in a list of observations corresponding to each SOM pattern. From this list of observations, various statistics can be calculated for each SOM pattern. The median, 10th, and 90th percentile inversion strengths for each SOM pattern are shown in Figure 9. On this figure

darker shading indicates a stronger median inversion. The largest median inversion strengths occur for patterns on the bottom left portion of the SOM, with median values up to 13.5°C. Slightly unstable conditions (median −0.3 to −0.1°C inversion strength) are found in the two patterns in the upper right portion of the SOM. Weakly stable conditions are found in the lower right portion of the SOM and moderate inversions are found in the top left corner of the SOM. The 10th and 90th percentile inversion strengths range from −0.8°C in the top right SOM pattern to 16.8°C in the bottom left SOM pattern.

The 10th and 90th percentile inversion strengths within each SOM pattern (Figure 9) provide an indication of the range of inversion strengths represented by each profile shown in Figure 3. The difference between the 10th and 90th percentile inversion strengths for individual SOM patterns ranges from 0.1 to 5.6°C and is smallest on the right side of the SOM and largest on the left side of the SOM. The range of inversion strengths within each pattern is roughly consistent with the difference in median inversion strength between adjacent SOM patterns indicating that the SOM is reasonably representing the intrapattern and interpattern differences present in the 100,000+ profile observations.

The frequency of occurrence of each pattern on the SOM can also be calculated from the list of observations associated with each pattern (Figure 10). On an annual basis the patterns in the rightmost column of the SOM occur almost 50% of the time indicating that near neutral conditions dominate at this site (Figure 10a). The frequency of occurrence of patterns is generally between 1 and 6% of the time, other than those in the rightmost SOM column, which occur more frequently. During the summer (Figure 10b), the two unstable patterns in the top right corner of the SOM occur almost 50% of the time, while individual patterns in the left two columns of the SOM occur less than 0.81% of the time, and the strongest inversion pattern (bottom left corner) occurs very rarely at 0.01% of the time. Some of the unstable patterns may be due to radiation errors, as discussed above, but as shown below, the weak wind shear and concave upward log wind profiles associated with these patterns suggest that the atmosphere is truly unstable for these patterns. In autumn (Figure 10c), the increasing stratification on the Ross Ice Shelf is evident as a shift of the most frequent patterns toward the lower right portion of the SOM. The six patterns in the bottom of the two rightmost columns of the SOM occur over 40% of the time, while the two unstable patterns in the top right corner of the SOM occur ~12% of the time. Patterns in the four leftmost columns of the SOM occur with frequencies ranging from 1.01 to 3.82%. Winter (Figure 10d) sees a continued increase in frequency of more stably stratified patterns, although the six weakly stable patterns in the lower right corner of the SOM still occur over 40% of the time. Patterns in the leftmost four columns of the SOM now occur with frequencies ranging from 1.11 to 6.92%. Of particular note are the relatively high frequencies for the most stable patterns in the lower left corner of the SOM, with the most stable pattern, in the lower left corner of the SOM, occurring 6.92% of the time. In spring (Figure 10e), weakening stability over the ice shelf is evident. The six patterns in the bottom right corner of the SOM still occur 40% of the time. The two unstable patterns in the top right of the SOM now occur over 16% of the time, while individual patterns in the leftmost four columns of the SOM occur from 1.01 to 5.05% with the strongest stability patterns (bottom left) occurring 2.27% of the time.

As indicated in the discussion above, the frequencies of the SOM patterns have a pronounced seasonal cycle (Figure 10f). The two unstable patterns at the top of the rightmost column of the SOM occur primarily in summer and spring. The slightly stable patterns in the lower right portion of the SOM tend to occur most often during autumn, winter, and spring, as do the strongly stable patterns on the left side of the SOM. The moderate stability patterns in the middle two columns of the SOM as well as the near neutral patterns in the middle of the two rightmost columns of the SOM tend to occur with near constant frequency throughout the year.

The relationship between the SOM potential temperature anomaly profiles and other characteristics of the near-surface atmosphere at the Tall Tower site can be explored by calculating statistics of other AWS observations for each SOM pattern. The median, 10th, and 90th percentile wind speeds at the lowest tower level for the entire 2 year period is shown in Figure 11a. The three most stable patterns, in the lower left corner of the SOM, are associated with the weakest winds (median less than 1.2 $m\,s^{-1}$). For the moderate stability patterns, in the top left and central columns of the SOM, more moderate winds (median 1.6 to 5.4 $m\,s^{-1}$) are observed. The strongest winds (median 6.3 to 7.2 $m\,s^{-1}$) occur for the nearly well mixed, slightly stable patterns found in the lower right portion of the SOM. Somewhat weaker winds (3.3 to 5.3 $m\,s^{-1}$) are associated with the slightly unstable patterns in the top right portion of the SOM. The range (10th to 90th

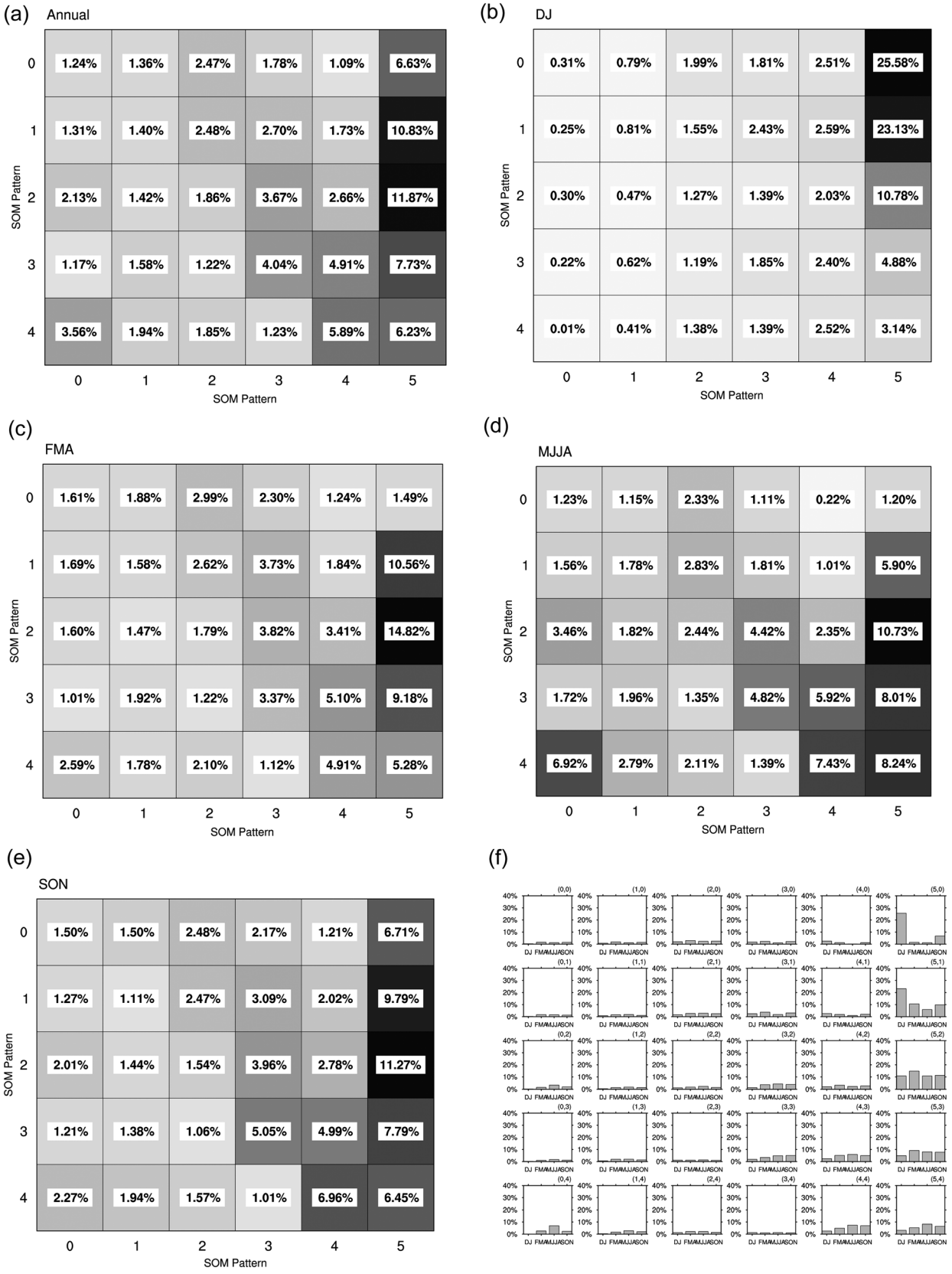

Figure 10. (a) Annual and seasonal ((b) DJ, (c) FMA, (d) MJJA, and (e) SON) frequency of occurrence of each SOM pattern. Darker shading indicates patterns that occur more frequently. (f) Histogram of seasonal frequency of occurrence of SOM patterns. Frequencies are plotted as a percentage of all days in a given season.

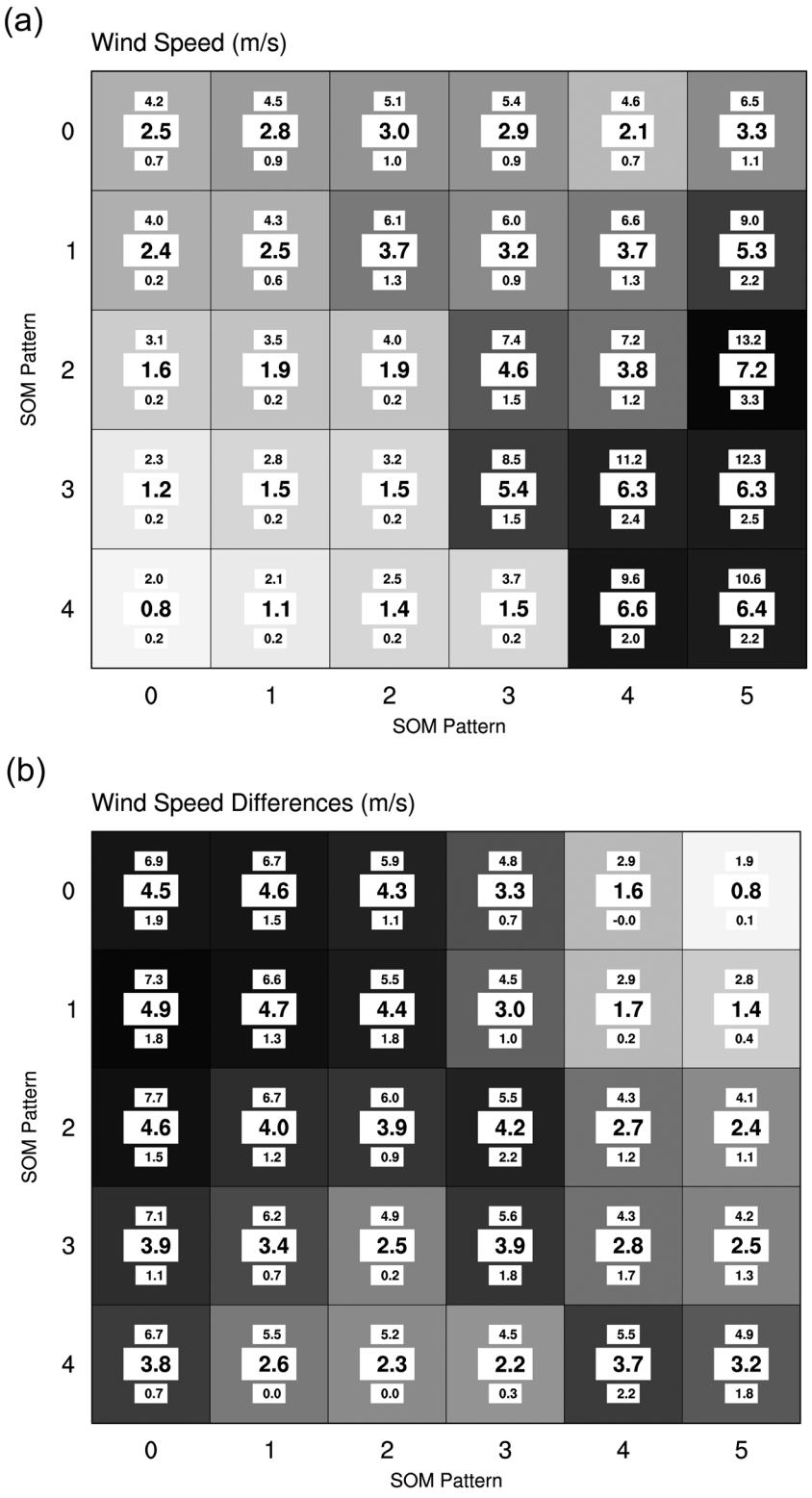

Figure 11. Median, 10th, and 90th percentile (a) lowest tower level wind speed and (b) wind speed difference over the depth of the tower (29.75 to 1.34 m) for each SOM pattern. Darker shading indicates larger median values. The 10th and 90th percentile values are listed below and above the median values, respectively.

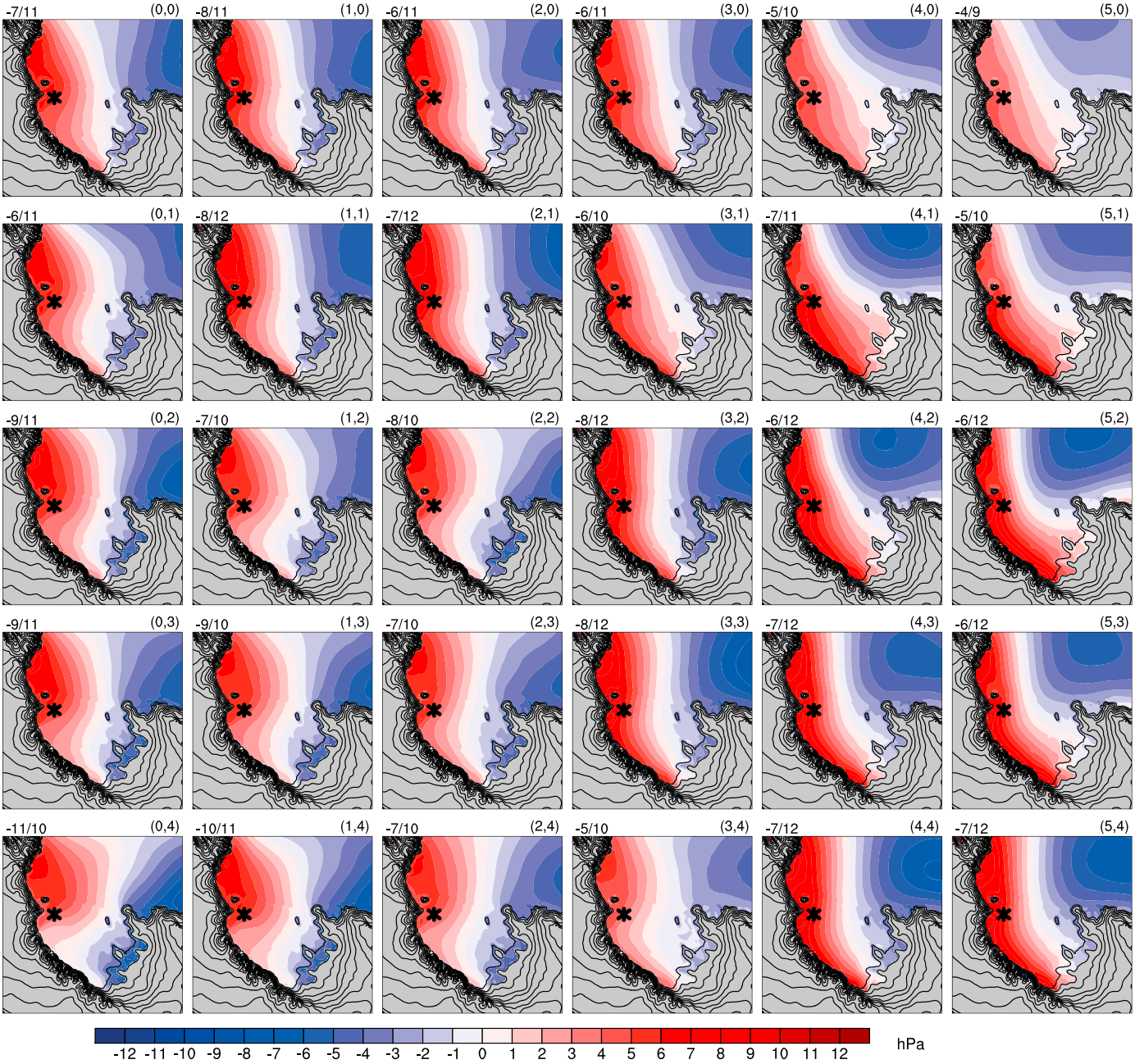

Figure 12. Pattern mean sea level pressure anomaly from Antarctic Mesoscale Prediction System 12 to 21 h forecasts. The asterisk in each panel marks the location of the Tall Tower AWS.

percentile) of wind speeds associated with each SOM pattern varies from 1.8 m s^{-1} (lower left portion of SOM) to 9.9 m s^{-1} (middle right portion of SOM). In general, a wider range of wind speeds occurs for SOM patterns with higher median wind speeds. SOM patterns with light winds, found in the bottom left corner of SOM, generally have light wind conditions most of the time, with 90th percentile wind speeds of up to 2.8 m s^{-1}. SOM patterns with strong winds, found in the lower right corner of the SOM, have 90th percentile wind speeds in excess of 10 m s^{-1} but do occasionally have light winds (10th percentile wind speeds of 2 m s^{-1}).

The average large-scale synoptic setting, as depicted by sea level pressure (SLP), for each of the SOM potential temperature profile patterns is shown in Figure 12. Following previous Antarctic synoptic analyses [e.g.,

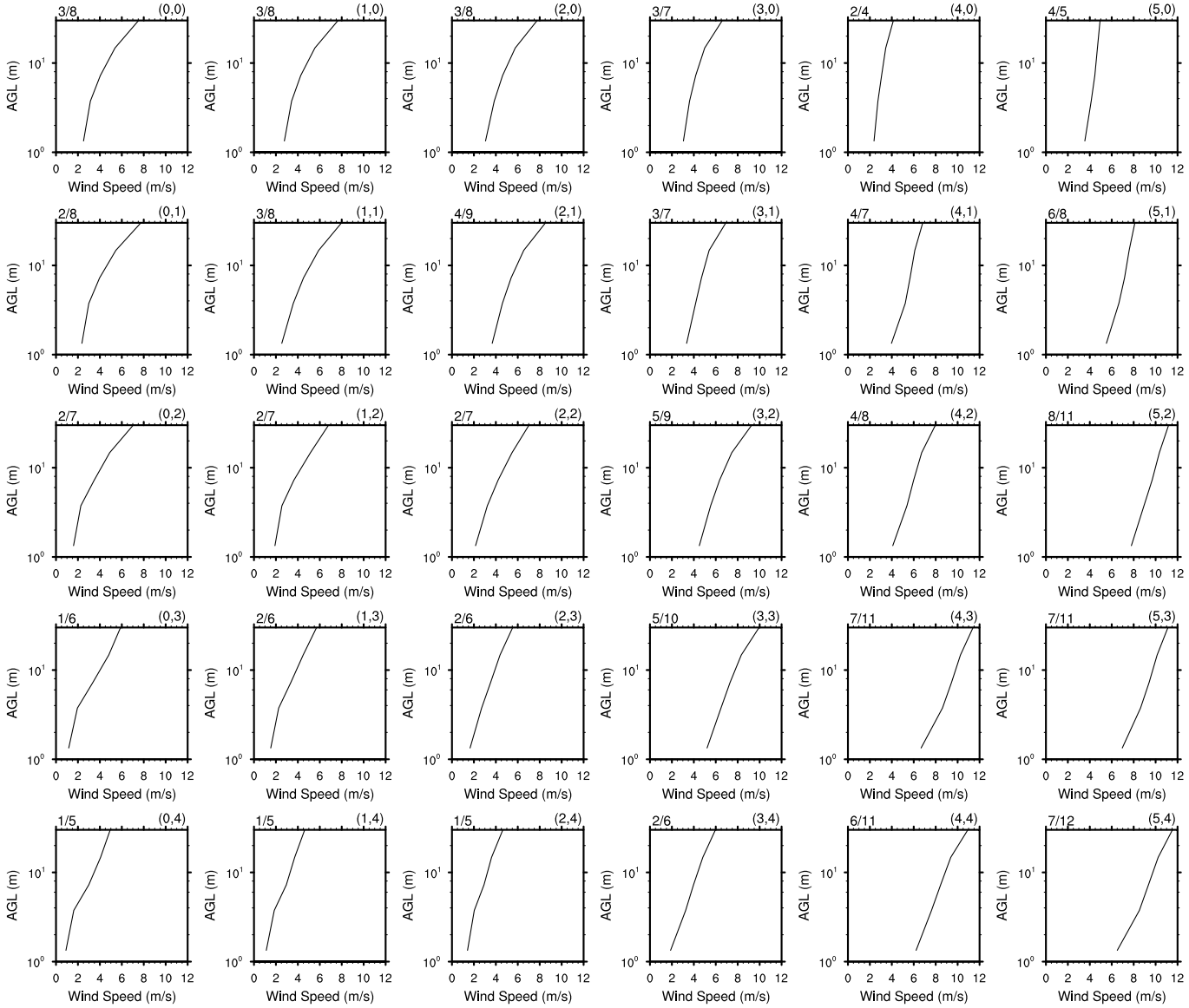

Figure 13. Pattern mean wind profiles plotted as a function of log height.

Nigro and Cassano, 2014, and references therein], forecasts (12 to 21 h) from the Antarctic Mesoscale Prediction System (AMPS) [*Powers et al*., 2012] for each time period corresponding to observations mapping to each SOM pattern were used to calculate the average SLP for each SOM pattern. The SLP patterns shown here are consistent with the wind speeds shown in Figure 11a. The weakly stable patterns in the bottom right corner of the SOM, associated with the strongest winds, are associated with the strongest pressure gradient and a SLP pattern consistent with a Ross Ice Shelf airstream (RAS) event [*Seefeldt and Cassano*, 2012; *Nigro and Cassano*, 2014]. The more stable patterns on the left side of the SOM are associated with a pronounced ridge extending from the Transantarctic Mountains toward the Tall Tower AWS, resulting in light winds that favor the development of strong inversion conditions at this site.

The median, 10th, and 90th percentile difference in wind speed over the depth of the tower is shown in Figure 11b. The smallest difference in wind speed over the depth of the tower (0.8 to 1.4 m s^{-1}) occurs for the two unstable patterns in the top right corner of the SOM. This is consistent with the unstable stratification and resultant vertical mixing reducing the wind shear over the depth of the tower and suggests that the unstable conditions found for these patterns are not an artifact of radiation errors in the temperature data.

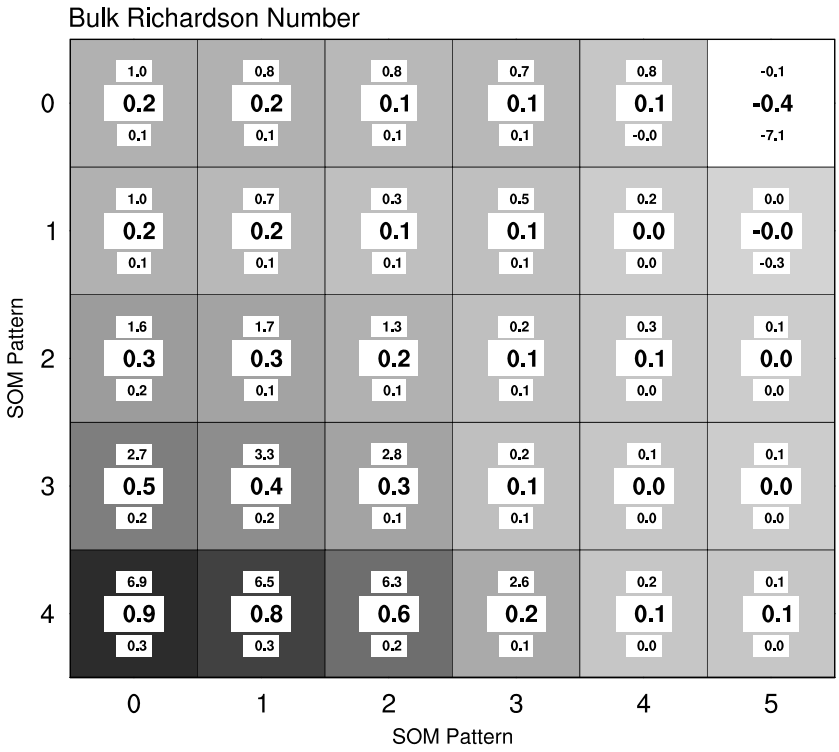

Figure 14. Median, 10th, and 90th percentile gradient Richardson number for each SOM pattern. Darker shading indicates larger median values. The 10th and 90th percentile values are listed below and above the median values, respectively.

More moderate wind speed differences (2.4 to 3.7 m s^{-1}) are found for patterns in the bottom right portion of the SOM. The larger wind shear in these patterns is consistent with the faster wind speeds found in these patterns (Figure 11a). The largest wind speed differences (3.9 to 4.9 m s^{-1}) occur for patterns in the top left portion of the SOM. The larger shear for these patterns occurs despite the weaker winds at the lowest level of the tower and reflects the decoupling of the winds over the depth of the tower. More moderate wind speed differences (2.6 to 3.9 m s^{-1}) are found for the most stable patterns, in the lower left corner of the SOM. These moderate wind shear values occur despite very light surface winds and are also consistent with decoupling of the winds over the depth of the tower for these very stable patterns.

Wind profiles plotted as a function of log height provide additional insight into the relationship between the observed winds and stability at the Tall Tower AWS (Figure 13). For neutral conditions, the log wind profile within the surface layer is expected to be linear. The profile will be concave upward for unstable conditions and concave downward for stable conditions [*Stull*, 1988, p 377]. The log wind profiles in the top two patterns in the two rightmost columns of the SOM are concave upward consistent with unstable conditions and suggest that the unstable conditions found for these patterns are not an artifact of radiation errors in the temperature data. The log wind profiles for patterns from the top left to bottom right corner of the SOM are generally concave downward, consistent with the stable stratification in these patterns. The log wind profiles in the lower left portion of the SOM do not exhibit a smooth profile but instead have a sharp kink at intermediate levels. The lack of a smooth log wind profile is indicative of the tower extending above the depth of the surface layer and is consistent with the large wind shear seen in these weak wind patterns (Figure 11b) resulting from a decoupling between the surface and upper levels of the tower due to the very strong inversion present in these patterns (Figure 4).

The median, 10th, and 90th percentile gradient Richardson numbers (Ri_b) for each SOM pattern are shown in Figure 14. Negative median Ri_b values are found for the two SOM patterns in top right corner of the SOM. Small positive (0.1) or zero median values of Ri_b are associated with the remaining patterns in the rightmost two columns of the SOM, consistent with the weak stability present in these patterns. Larger values (0.1 to 0.3) of Ri_b occur in the upper left portion of the SOM and the largest values (0.5 to 0.9) are found in the lower

left portion of the SOM, reflecting the greater stability of these patterns. The 10th and 90th percentile Ri_b values range from −7.1 (top right SOM pattern) to 6.9 (bottom left SOM pattern).

5. Discussion and Conclusion

Over the period February 2011 to January 2013 the potential temperature at the Tall Tower AWS ranged from −56.8°C to 2.0°C with an annual range of monthly median potential temperature of 28°C (Figure 4a). The potential temperature exhibited a classic Antarctic coreless winter with monthly median temperatures varying little from April to September. The maximum wind speed observed over the 2 year period was 21.4 m s^{-1} at 1.34 m, with monthly median wind speeds generally strongest in the nonsummer months (Figure 4b).

Analysis of the annual, seasonal, and diurnal mean atmospheric state at the Tall Tower AWS indicated that a significant diurnal cycle in potential temperature occurs only at the two lowest tower levels (0.85 and 1.83 m) during summer (Figure 5). The mean diurnal cycle ranged from 0.5 to 4.0°C at the 0.85 m level and from 0.4 to 2.4°C at the 29.75 m level (Figure 5).

Stable conditions dominate at this site, occurring 83% of the time (Figure 6). The strongest inversions over the depth of the tower exceed 25°C. Neutral to unstable conditions were observed throughout the year, occurring 17% of the time annually. Weakly unstable conditions occur 50% of the time during the summer (Figure 6b). Stable stratification was the dominant stability class (84 to 94% of the time) for the remaining three seasons (Figures 6c to 6e). In the annual mean stable stratification over the depth of the tower persists throughout the diurnal cycle (Figure 7). During the summer and spring unstable stratification occurs for a portion of the mean diurnal cycle between the two lowest tower levels, while stable stratification persists throughout the diurnal cycle in fall and winter.

A strong relationship between wind speed and inversion strength was found (Figure 8). The strongest inversions were observed when the wind speed was less than 4 m s^{-1} and the inversion strength rapidly decreased as the wind speed increased above 4 m s^{-1}. The rapid weakening of inversion strength, and thus warming of the near-surface air, is consistent with previous modeling [*Lüpkes et al*., 2008] and observational [*Riordan*, 1977; *Steinhoff et al*., 2009; *Rinke et al*., 2012] studies in both the Arctic and Antarctic, that found near-surface temperature increased at a wind speed threshold of anywhere from 2 to 6 m s^{-1}. The 10th percentile inversion strengths were near neutral, or even slightly unstable, for all wind speeds throughout the year (Figure 8).

The SOM clustering technique allowed the more than 100,000 observed potential temperature profiles to be represented by just 30 SOM profile patterns (Figure 3). The 30 SOM patterns ranged from slightly unstable to strongly stable conditions. The median SOM pattern inversion strengths ranged from −0.3 to 13.5°C (Figure 9). The nearly well mixed profiles, found on the right side of the SOM, were the most common potential temperature profiles throughout the year (Figure 10a). During the summer (Figure 10b) the unstable patterns, in the top right corner of the SOM, occurred almost 50% of the time. The weakly stable patterns, found in the lower right corner of the SOM, occurred more than 40% of the time during autumn, winter, and spring. The strongest inversion pattern (lower left corner of the SOM) occurred 0.01% of the time in summer but occurred 6.92% of the time in winter. While the patterns on the right side of the SOM (Figure 3) appear almost identical they do represent different atmospheric conditions with unstable profiles depicted in the top right portion of the SOM and slightly stable conditions depicted in the bottom right portion of the SOM. These physically different states are also revealed by differences in wind speed, wind speed difference over the depth of the tower, and the shape of the log wind profiles for these patterns.

The observed winds (Figures 11 and 13) showed clear relationships with the different potential temperature profiles represented by the SOM (Figure 3). The strongest inversion patterns (lower left corner of the SOM) occurred with median wind speeds < 1.5 m s^{-1}. The nearly well mixed but slightly stable profiles (lower right corner of the SOM) occurred with median wind speeds > 6.0 m s^{-1}. The wind speed shear was smallest for the unstable patterns found in the top right corner of the SOM, consistent with convective mixing occurring when these profiles were observed. The largest wind speed shear was found for the moderate stability profiles (top left corner of the SOM). This was attributed to the moderate wind speeds occurring for these profile types combined with decoupling between the surface and upper levels of the tower in the presence of moderate inversion conditions. While instrument and radiation errors may impact the inversion strengths

presented here the physically consistent results between the SOM-identified potential temperature profiles and winds suggest that even the small vertical potential temperature differences found in the right two columns of the SOM are in fact accurately resolved. The two unstable patterns in the top right corner of the SOM occur with light winds that would be necessary to create superadiabatic conditions near the surface. In addition, these patterns also exhibit weak wind shear and concave upward log wind profiles (Figure 13) consistent with unstable conditions. The near neutral to slightly stable patterns (bottom right corner of the SOM) occur when stronger winds are observed. With these stronger winds it is unlikely that surface heating would be able to maintain a superadiabatic lapse rate near the surface but turbulence driven by the strong winds would result in the very weak vertical potential temperature gradients observed in these patterns. This physical consistency also suggests that the SOM-based partitioning of the over 100,000 potential temperature profiles is producing results that are physically meaningful and highlights the potential benefits of using SOMs to meaningfully stratify large boundary layer data sets.

The log wind profiles (Figure 13) were consistent with theoretical expectations with linear log wind profiles found for neutral conditions, concave upward log wind profiles for unstable conditions (top right corner of SOM), and concave downward log wind profiles for stable conditions (top left to bottom right corner of SOM). The gradient Richardson number varied from slightly unstable (−0.4) for patterns in the top right corner of the SOM to strongly stable (0.9) for patterns in the bottom left corner of the SOM (Figure 14).

Comparison of the Tall Tower AWS observations with other tower observations from the polar regions reveals many similarities as well as some notable differences. *Hudson and Brandt* [2005] noted a lack of a diurnal cycle in temperature at the South Pole, while *Genthon et al*. [2013] found a pronounced diurnal cycle at the lowest tower levels but not at the upper (43.4 m) tower level at Dome C. *Riordan* [1977] noted a clear diurnal cycle at all tower levels at Plateau Station during February and March. At the Tall Tower AWS there was a significant diurnal cycle only at the two lowest tower levels in summer, consistent with the results from all but the South Pole tower [*Hudson and Brandt*, 2005]. The lack of a diurnal cycle at the South Pole is not unexpected given the constant solar elevation angle throughout the diurnal cycle at this location.

Several of the polar tower observations summarized in the introduction found near neutral or unstable conditions during the summer [*Persson et al*., 2002; *Genthon et al*., 2013; *van Dam et al*., 2013] consistent with our findings at the Tall Tower AWS. At the South Pole, *Hudson and Brandt* [2005] found that inversion conditions occur 75% of the time during the summer, while at the Tall Tower AWS we find inversion conditions occur only 50% of the time during the summer. In winter, stable conditions are observed at South Pole and Tall Tower with a similar frequency of near 90%. SHEBA observations indicate that stable conditions dominate during the winter but near neutral conditions can occur at anytime of the year. During the winter at SHEBA the weaker stability was associated with increased cloud cover or increased wind speed [*Persson et al*., 2002]. Observations from the Tall Tower AWS also indicate near neutral stability occurring throughout the year. The data from the Tall Tower AWS are not sufficient to assess changes in cloud cover, but we do find that increased wind speed at this site is associated with near neutral stability throughout the year, consistent with the SHEBA results. At Plateau Station [*Riordan*, 1977] and South Pole [*Hudson and Brandt*, 2005] the strongest inversions occurred at moderate wind speeds of a few meters per second consistent with our findings at the Tall Tower AWS on the Ross Ice Shelf and consistent with other modeling [*Lüpkes et al*., 2008] and observational studies [*Steinhoff et al*., 2009; *Rinke et al*., 2012] in the polar regions. At South Pole and Dome C, the winter inversion strength was typically 0.5 to 1.0°C m^{-1} [*Hudson and Brandt*, 2012; *Genthon et al*., 2013], while at the Tall Tower AWS the median winter inversion strength is 0.1°C m^{-1}. The weaker inversion at Tall Tower is likely attributable to the stronger winds on the Ross Ice Shelf during the winter than at Dome C or South Pole, and the stronger radiative cooling that can occur over the high Antarctic plateau at Dome C and South Pole.

The Tall Tower AWS data provide observations of the near-surface atmosphere from a portion of Antarctica that previously lacked any above surface observations. As such this data set is likely to be of value for many future studies and several additional studies using these data are already underway or planned. The Tall Tower observations are currently being used to evaluate Antarctic Mesoscale Prediction System (AMPS) [*Powers et al*., 2012] forecasts of the lowest portion of the Antarctic atmosphere. Following test deployments in 2012 [*Cassano*, 2014], Small Unmanned Meteorological Observer (SUMO) unmanned aerial vehicles were used in a 2 week field campaign in January 2014 to observe the entire depth of the boundary layer at the

Tall Tower AWS site. During this field campaign, a total of 41 SUMO flights were completed that documented the diurnal evolution of the boundary layer on six flight days.

The results presented here represent an initial assessment of the near-surface climate at the Tall Tower AWS and many of the results presented above could be explored in greater detail with an emphasis on the processes responsible for creating the observed features. In particular, measurements of surface radiative fluxes would be of great value in understanding the processes that control the near-surface stability at this site. While observations of net shortwave and longwave radiation are available from the Tall Tower AWS an initial assessment of these data indicate that careful quality control of this data will be needed before it can be used.

This paper has demonstrated the use of self-organizing maps (SOMs) for stratifying large boundary layer data sets in an objective and physically meaningful way. Other applications of SOMs can be envisioned for boundary layer studies including model evaluation studies that assess model performance for different SOM-identified boundary layer regimes or SOM-based analyses of boundary layer wind profiles and low level jets. The latter could be particularly useful for wind power meteorology studies.

Acknowledgments
This work was funded by the United States National Science Foundation grants ANT-0943952, ANT-0944018, ANT-1245663, and ANT-1245737. The authors thank the many people associated with the United States Antarctic Program that provided the logistic support for this effort. We thank the four reviewers for their time and useful comments which helped improve this manuscript. The Tall Tower AWS data used for this analysis are available from http://amrc.ssec.wisc.edu.

References

Anderson, P. S. (2009), Measurement of Prandtl number as a function of Richardson number avoiding self-correlation, *Boundary Layer Meteorol.*, *131*, 345–362.
Bowen, B. M. (2000), Near-neutral surface layer turbulence at the Boulder atmospheric observatory tower: Evidence of increasing vertical turbulence with height, *J. Appl. Meteorol.*, *39*, 716–724.
Bromwich, D. H. (1988), Snowfall in high southern latitudes, *Rev. Geophys.*, *26*, 149–168, doi:10.1029/RG026i001p00149.
Bromwich, D. H., et al. (2012), Tropospheric clouds in Antarctica, *Rev. Geophys.*, *50*, RG1004, doi:10.1029/2011RG000363.
Cassano, E. N., J. M. Glisan, J. J. Cassano, W. J. Gutowski Jr., and M. W. Seefeldt (2015), Slef-organizing map analysis of widespread temperature extremes in Alaska and Canada, *Clim. Res.*, *62*, 199–218, doi:10.3354/cr01274.
Cassano, J. J. (2014), Observations of atmospheric boundary layer temperature profiles with a small unmanned aerial vehicle, *Antarct. Sci.*, *26*, 205–213, doi:10.1017/S0954102013000539.
Comiso, J. C. (1994), Surface temperatures in the polar regions from Nimbus 7 temperature humidity infrared radiometer, *J. Geophys. Res.*, *99*, 5181–5200, doi:10.1029/93JC03450.
Genthon, C., M. S. Town, D. Six, V. Favier, S. Argentini, and A. Pellegrini (2010), Meteorological atmospheric boundary layer measurements and ECMWF analyses during summer at Dome C, Antarctica, *J. Geophys. Res.*, *115*, D05104, doi:10.1029/2009JD012741.
Genthon, C., D. Six, V. Favier, M. Lazzara, and L. Keller (2011), Atmospheric temperature measurement biases on the Antarctic plateau, *J. Atmos. Oceanic Technol.*, *28*, 1598–1605, doi:10.1175/JTECH-D-11-00095.1.
Genthon, C., D. Six, H. Gallee, P. Grigioni, and A. Pellegrini (2013), Two years of atmospheric boundary layer observations on a 45-m tower at Dome C on the Antarctic plateau, *J. Geophys. Res. Atmos.*, *118*, 3218–3232, doi:10.1002/jgrd.50128.
Grachev, A. A., C. W. Fairall, P. O. G. Persson, E. L. Andreas, and P. S. Guest (2005), Stable boundary-layer scaling regimes: The SHEBA data, *Boundary Layer Meteorol.*, *116*, 201–235.
Grachev, A. A., E. L. Andreas, C. W. Fairall, P. S. Guest, and P. O. G. Persson (2012), Outlier problem in evaluating similarity functions in the stable atmospheric boundary layer, *Boundary Layer Meteorol.*, *144*, 137–155.
Grachev, A. A., E. L. Andreas, C. W. Fairall, P. S. Guest, and P. O. G. Persson (2013), The critical Richardson number and limits of applicability of local similarity theory in the stable boundary layer, *Boundary Layer Meteorol.*, *147*, 51–82.
Hewitson, B. C., and R. G. Crane (2002), Self-organizing maps: Applications to synoptic climatology, *Clim. Res.*, *22*, 13–26.
Horiguchi, M., T. Hayashi, A. Adachi, and S. Onogi (2012), Large-scale turbulence structures and their contributions to the momentum flux and turbulence in the near-neutral atmospheric boundary layer observed from a 213-m tall meteorological tower, *Boundary Layer Meteorol.*, *144*, 179–198.
Hudson, S. R., and R. E. Brandt (2005), A look at the surface-based temperature inversion on the Antarctic plateau, *J. Clim.*, *18*, 1673–1696, doi:10.1175/JCLI3360.1.
Jones, D. A., and I. Simmonds (1993), A climatology of Southern Hemisphere extratropical cyclones, *Clim. Dyn.*, *9*, 131–145.
King, J. C., and P. S. Anderson (1988), Installation and performance of the stable instrumentation at Halley, *British Antarct. Surv. Bull.*, *79*, 65–77.
King, J. C., and J. Turner (1997), *Antarctic Meteorology and Climatology*, 409 pp., Cambridge Univ. Press, Cambridge.
King, J. C., S. D. Mobbs, J. M. Rees, P. S. Anderson, and A. D. Culf (1989), The STABLE Antarctic boundary layer experiment at Halley Base, *Weather*, *44*, 398–405.
Kohonen, T. (2001), *Self-organizing Maps*, 501 pp., Springer, New York.
Lazzara, M. A., G. A. Weidner, L. M. Keller, J. E. Thom, and J. J. Cassano (2012), Antarctic automatic weather station program: 30 years of polar observations, *Bull. Am. Meteorol. Soc.*, *93*, 1519–1537, doi:10.1175/BAMS-D-11-00015.1.
Lettau, B. (1969), The transport of moisture into the Antarctic interior, *Tellus*, *21*, 331–340.
Lüpkes, C., T. Vihma, G. Birnbaum, and U. Wacker (2008), Influence of leads in sea ice on temperature of the atmospheric boundary layer during polar night, *Geophys. Res. Lett.*, *35*, L03805, doi:10.1029/2007GL032461.
Mahrt, L. J., and W. Schwerdtfeger (1970), Ekman spirals for exponential thermal wind, *Boundary Layer Meteorol.*, *1*, 137–145.
Munoz, R. C., M. J. Falvey, M. Araya, and M. Jacques-Coper (2013), Strong down-valley low-level jets over the Atacama desert: Observational characterization, *J. Appl. Meteorol. Climatol.*, *52*, 2735–2752.
Nigro, M. A., and J. J. Cassano (2014), Identification of surface wind patterns over the Ross Ice Shelf, Antarctica using self-organizing maps, *Mon. Weather Rev.*, *142*, 2361–2378, doi:10.1175/MWR-D-13-00382.1.
Parish, T. R., and D. H. Bromwich (1987), The surface windfield over the Antarctic ice sheets, *Nature*, *328*, 51–54.
Parish, T. R., and D. H. Bromwich (2007), Reexamination of the near-surface airflow over the Antarctic continent and implications on atmospheric circulations at high southern latitudes, *Mon. Weather Rev.*, *135*, 1961–1973, doi:10.1175/MWR3374.1.

Parish, T. R., D. H. Bromwich, and R. Y. Tzeng (1994), On the role of the Antarctic continent in forcing large-scale circulations in the high southern latitudes, *J. Atmos. Sci.*, *51*, 3566–3579, doi:10.1175/1520-0469(1994)051<3566:OTROTA>2.0.CO;2.

Persson, P. O. G., C. W. Fairall, E. L. Andreas, P. S. Guest, and D. K. Perovich (2002), Measurements near the Atmospheric Surface Flux Group tower at SHEBA: Near-surface conditions and surface energy budget, *J. Geophys. Res.*, *107*(C10), 8045, doi:10.1029/2000JC000705.

Phillpot, H. R., and J. W. Zillman (1970), The surface temperature inversion over the Antarctic continent, *J. Geophys. Res.*, *75*, 4161–4169, doi:10.1029/JC075i021p04161.

Powers, J. G., K. W. Manning, D. H. Bromwich, J. J. Cassano, and A. M. Cayette (2012), A decade of Antarctic science support through AMPS, *Bull. Am. Meteorol. Soc.*, *93*, 1699–1712, doi:10.1175/BAMS-D-11-00186.1.

Rinke, A., Y. Ma, L. Bian, Y. Xin, K. Dethloff, P. O. G. Person, C. Lüpkes, and C. Xiao (2012), Evaluation of atmospheric boundary layer-surface process relationships in a regional climate model along an East Antarctic traverse, *J. Geophys. Res.*, *117*, D09121, doi:10.1029/2011JD016441.

Riordan, A. J. (1977), Variations of temperature and air motion in the 0- to 32-meter layer at Plateau Station, Antarctica, in *Meteorological Studies at Plateau Station, Antarctica*, *Antarctic Res. Ser.*, vol. 25, edited by J. A. Businger, pp. 113–127, AGU, Washington D. C.

Schwerdtfeger, W. (1977), Temperature regime of the South Pole: Results of 20 years' observations at Amundsen-Scott Station, *Antarct. J. U. S.*, *12*, 156–159.

Schwerdtfeger, W. (1984), *Weather and Climate of the Antarctic*, 261 pp., Elsevier, Amsterdam.

Seefeldt, M. W., and J. J. Cassano (2008), An analysis of low-level jets in the greater Ross Ice Shelf region based on numerical simulations, *Mon. Weather Rev.*, *136*, 4188–4205.

Seefeldt, M. W. and J. J. Cassano (2012), A description of the Ross Ice Shelf air stream (RAS) through the use of self-organizing maps (SOMs), *J. Geophys. Res.*, *117*, D09112, doi:10.1029/2011JD016857.

Sorbjan, Z., and A. Czerwinska (2013), Statistics of turbulence in the stable boundary layer affected by gravity waves, *Boundary Layer Meteorol.*, *148*, 73–91.

Steinhoff, D. F., S. Chaudhuri, and D. H. Bromwich (2009), A case study of a the Ross Ice Shelf airstream event: A new perspective, *Mon. Weather Rev.*, *137*, 4030–4046, doi:10.1175/2009MWR2880.1.

Stull, R. B. (1988), *An Introduction to Boundary Layer Meteorology*, 666 pp., Kluwer Acad., Dordrecht.

Summerhayes, C. P. (2008), International collaboration in Antarctica: The International Polar Years, the International Geophysical Year, and the Scientific Committee on Antarctic Research, *Polar Rec.*, *44*, 321–334, doi:10.1017/S0032247408007468.

Van Dam, B., D. Helmig, W. Neff, and L. Kramer (2013), Evaluation of boundary layer depth estimates at Summit Station, Greenland, *J. Appl. Meteorol. Climatol.*, *52*, 2356–2362.

Van Ulden, A. P., and J. Wieringa (1996), Atmospheric boundary layer research at Cabauw, *Boundary Layer Meteorol.*, *78*, 39–69.

Whiteman, C. D., X. Bian, and J. L. Sutherland (1999), Wintertime surface wind patterns in the Colorado River valley, *J. Appl. Meteorol.*, *38*, 1118–1130.